

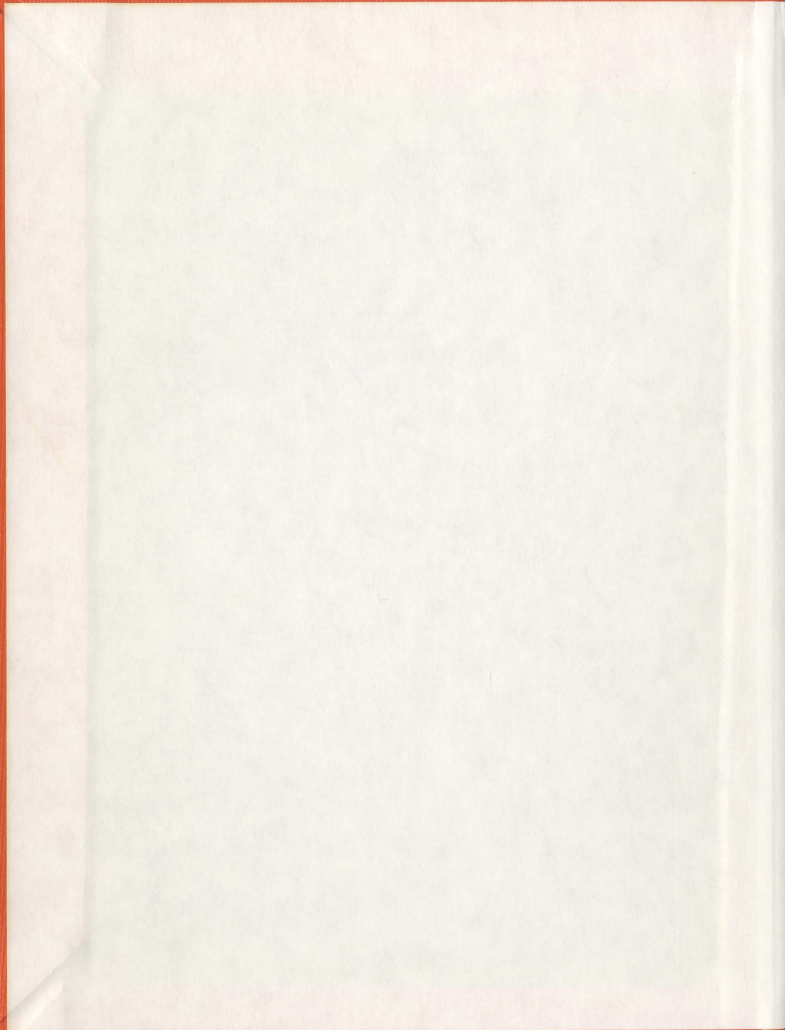
UNDERWATER ACOUSTIC SWEPT  
CARRIER COMMUNICATIONS

CENTRE FOR NEWFOUNDLAND STUDIES

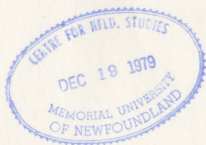
**TOTAL OF 10 PAGES ONLY  
MAY BE XEROXED**

(Without Author's Permission)

ROBERT LESLIE BARBOUR



010296







Copy 3

UNDERWATER ACOUSTIC SWEEP CARRIER  
COMMUNICATIONS

by

Robert Leslie Barbour, B. Eng.



Faculty of Engineering  
Memorial University of Newfoundland  
April, 1979

St. John's

Newfoundland

## ABSTRACT

Underwater acoustic communication is severely affected by multipath interference. A novel idea based on the observation that the time separation between direct and multipath signals can be utilized to suppress multipath interference is developed in this thesis.

A proposed system employs a carrier with instantaneous frequency swept periodically in time over a broad frequency range. The carrier is narrowband modulated by a message signal resulting in a time varying instantaneous spectrum of the transmitted signal. The received signal is demodulated by a bandpass tracking receiver. The low sweeping frequency determines the multipath spectrum and the degree of multipath suppression by the tracking bandpass receiver.

Computer evaluation of the swept carrier concept together with lab and field tests conducted on a system prototype show conclusively that swept carrier communication is a feasible technique for multipath interference suppression.

## ACKNOWLEDGEMENTS

The author wishes to thank his supervisor, Dr. A. Zielinski for his guidance, encouragement and help in all stages of this project.

Thanks go to the Ocean Engineering Department of Memorial for providing the necessary sea trial time in which the system prototype could be tested.

The author wishes to acknowledge the financial assistance provided by the Centre for Cold Ocean Resources Engineering (C-CORE) during the period from September 1976 to August 1978 through the C-CORE Fellowship program.

Finally, thanks to Mrs. Lorraine Bugden for her patience in typing this thesis.

# TABLE OF CONTENTS

	Page
ABSTRACT	i
ACKNOWLEDGEMENTS	ii
TABLE OF CONTENTS	iii
LIST OF TABLES	v
LIST OF FIGURES	vi
LIST OF SYMBOLS	x
CHAPTER I INTRODUCTION	1
1.1 Underwater Communications and Acoustics	1
CHAPTER II MODEL OF THE UNDERWATER ACOUSTIC CHANNEL	7
2.1 Introduction	7
2.2 Model Formulation	7
2.3 Impulse Response of the Model	11
2.4 Response of the Model to a Harmonic Signal	11
CHAPTER III SWEPT CARRIER COMMUNICATIONS	18
3.1 Introduction	18
3.2 Swept Carrier Communications	18
CHAPTER IV COMPUTER EVALUATION OF THE SWEPT CARRIER SYSTEM PERFORMANCE	26
4.1 Introduction	26
4.2 Computer Simulation Results	27
CHAPTER V SWEPT CARRIER SYSTEMS	46
5.1 Introduction	46
5.2 Functional Structure of a Swept Carrier System	46
5.3 Swept Carrier Amplitude Modulation	48
5.4 Swept Carrier Frequency Modulation	49

CHAPTER VI	PROTOTYPE IMPLEMENTATION AND TESTING	50
6.1	Introduction	50
6.2	Swept Carrier Multipath Channel Simulator	52
6.3	Laboratory Tests	54
6.4	Tank and Sea Experiments	62
CHAPTER VII	CONCLUSIONS AND FURTHER WORK	70
BIBLIOGRAPHY AND REFERENCES		72
Appendix A	Computer Program Associated with Chapter IV	77
Appendix B	Design Considerations of Experimental System Receiver	88
Appendix C	Related Schematics and Specifications associated with System Prototype	92

# LIST OF TABLES

	Page
Table 4.1 Computer Simulation Results showing the Dependence of P on $\phi$	35
Table 4.2 Computer Simulation Results showing the Dependence of P on $\omega_v T$	43
Table 4.3 Computer Simulation Results showing the Dependence of P on $2\Delta\omega_v/B_r$	45
Table 6.1 Lab Results showing the Dependence of P on $\phi$	59



# LIST OF FIGURES

		Page
Figure 1.1a	The Attenuation of Electromagnetic Waves in Clear Sea Water	3
Figure 1.1b	The Attenuation of Sound in Sea and Fresh Water as a function of Frequency	3
Figure 1.2	Underwater Acoustic Communication Link	5
Figure 2.1	An Underwater Communication System Model	8
Figure 2.2	Impulse Response of the Channel Model	12
Figure 2.3	Decay of Reverberation Intensity	13
Figure 2.4	The Effect of Geometry on the Received Signal Structure	14
Figure 2.5	Phasor Representation for the Direct and Multipath Signals	16
Figure 3.1	Instantaneous Spectra of the Direct and Multipath Signals	20
Figure 3.2	Phasor Representation of the Swept Carrier Concept for $F_d(\omega, t)$ and $F_m(\omega, t)$	23
Figure 4.1a	Computer Simulation: $p(t)$ vs time for one period of $v(t)$ for $\phi=0^\circ$	29
Figure 4.1b	Computer Simulation: $p(t)$ vs time for one period of $v(t)$ for $\phi=30^\circ$	30
Figure 4.1c	Computer Simulation: $p(t)$ vs time for one period of $v(t)$ for $\phi=90^\circ$	31
Figure 4.1d	Computer Simulation: $p(t)$ vs time for one period of $v(t)$ for $\phi=180^\circ$	32
Figure 4.1e	Computer Simulation: $p(t)$ vs time for one period of $v(t)$ for $\phi=270^\circ$	33
Figure 4.1f	Computer Simulation: $p(t)$ vs time for one period of $v(t)$ for $\phi=360^\circ$	34

Figure 4.2a	Computer Simulation: P vs $\omega_V \tau$ for $\omega_V T = 30^\circ$	37
Figure 4.2b	Computer Simulation: P vs $\omega_V \tau$ for $\omega_V T = 60^\circ$	37
Figure 4.2c	Computer Simulation: P vs $\omega_V \tau$ for $\omega_V T = 90^\circ$	38
Figure 4.2d	Computer Simulation: P vs $\omega_V \tau$ for $\omega_V T = 120^\circ$	38
Figure 4.2e	Computer Simulation: P vs $\omega_V \tau$ for $\omega_V T = 150^\circ$	39
Figure 4.2f	Computer Simulation: P vs $\omega_V \tau$ for $\omega_V T = 180^\circ$	39
Figure 4.2g	Computer Simulation: P vs $\omega_V \tau$ for $\omega_V T = 210^\circ$	40
Figure 4.2h	Computer Simulation: P vs $\omega_V \tau$ for $\omega_V T = 240^\circ$	40
Figure 4.2i	Computer Simulation: P vs $\omega_V \tau$ for $\omega_V T = 270^\circ$	41
Figure 4.2j	Computer Simulation: P vs $\omega_V \tau$ for $\omega_V T = 300^\circ$	41
Figure 4.2k	Computer Simulation: P vs $\omega_V \tau$ for $\omega_V T = 330^\circ$	42
Figure 4.2L	Computer Simulation: P vs $\omega_V \tau$ for $\omega_V T = 360^\circ$	42
Figure 4.3	Computer Simulation: P vs $2\Delta\omega_V/B_T$ for $\omega_V T = 30^\circ$ and $\omega_V T = 360^\circ$ for $\phi = 180^\circ$	44
Figure 5.1	The Functional Structure of the Swept Carrier System	47
Figure 6.1	Functional Block Diagram of a Phase- Locked Loop	51
Figure 6.2a	The Swept Carrier Multipath Channel Simulator	53
Figure 6.2b	Labratory Set-up of the Swept Carrier Multipath Channel Simulator	55
Figure 6.3	Lab Result: Recovered Sweeping Signal $v'(t)$ showing Distortion associated with Interferring Tone	56

Figure 6.4	Lab Result: Transmitted Message $x(t)$ (upper trace) and Recovered Message (lower trace) showing Distortion associated with Interfering Tone	56
Figure 6.5	Lab Result: Normalized Average Noise Power $P$ at the FM Demodulator Output vs Angle Separation $\phi$ for $M=10\text{kHz}$ , $30\text{kHz}$ and $100\text{kHz}$	58
Figure 6.6a	Lab Result: Recovered Sweeping Waveform $v'(t)$ for $\phi=0$ , $M=10\text{kHz}$	60
Figure 6.6b	Lab Result: Recovered Sweeping Waveform $v'(t)$ for $\phi=180$ , $M=10\text{kHz}$	60
Figure 6.7a	Lab Result: Recovered Message Signal $x'(t)$ for a Frequency Modulated Swept Carrier, $\phi=0$ , $\Delta M=10\text{kHz}$	61
Figure 6.7b	Lab Result: Recovered Message Signal $x'(t)$ for a Frequency Modulated Swept Carrier, $\phi=180$ , $\Delta M=10\text{kHz}$	61
Figure 6.8	Functional Block Diagram of System Prototype	63
Figure 6.9	Tank Tests: Transmitted (upper trace) and received (lower trace) signals	64
Figure 6.10	Tank Tests: Recovered sweeping waveform $v'(t)$	64
Figure 6.11	Geometry associated with Sea Trials	65
Figure 6.12	Sea Trials: Transmitted (upper trace) and Received (lower trace) signals	66
Figure 6.13a	Sea Trials: Received signal $r(t)$ (upper trace) and Recovered Sweeping Signal $v'(t)$ (lower trace) for $\phi=180$	68
Figure 6.13b	Sea Trials: Received Signal $r(t)$ (upper trace) and Recovered Sweeping Signal $v'(t)$ (lower Trace) for $\phi=110$	68
Figure 6.14a	Sea Trials: Recovered Message Signal for Swept Carrier Transmission, $\phi=180$	69
Figure 6.14b	Sea Trials: Recovered Message Signal for Classical FM Transmission	69
Figure A1	Flowchart for Computer Simulation Program	78

Figure B1	Model of a Second Order Phase-Locked Loop working as a Tracking Bandpass Filter and Frequency Demodulator	89
Figure B2	Amplitude Frequency Characteristic of a Second Order Loop with $F(j\omega) = (1+T_1j\omega)/(1+T_2j\omega)$	91
Figure C1	Sweep Generation	93
Figure C2	Message Generation	94
Figure C3	Carrier Generation	95
Figure C4	Power Amplification	96
Figure C5	Source Level of the Transmitting Transmitter	97
Figure C6	Typical free-field voltage sensitivity, the LC-10 hydrophone open-circuit voltage at end of 25-foot coaxial cable	98
Figure C7	Pre-amplification Stage No.2	99
Figure C8	Tracking Bandpass Filter and Frequency Demodulator	100
Figure C9	Audio Amplifier	101

# LIST OF SYMBOLS

$B_x$	- Message signal bandwidth
$B_r$	- Receiver's filter bandwidth
$d(t)$	- Direct path signal
$E$	- Expected value
$F(\omega, t)$	- Instantaneous Spectrum
$H(j\omega)$	- Time invariant transfer function
$H(\omega, t)$	- Time dependent real transfer function
$K(j\omega)$	- Time invariant transfer function of receiver's front filter
$K(\omega, t)$	- Time dependent real transfer function of receiver's front filter
$m(t)$	- Multipath signal
$M$	- Multipath spectrum width
$P$	- Normalized average output noise power
$p(t)$	- Normalized instantaneous output noise power
$r(t)$	- Received acoustic signal
$s(t)$	- Transmitted acoustic signal
$t$	- Time
$T$	- Multipath duration time
$v(t)$	- Sweeping waveform
$x(t)$	- Message signal
$\tau$	- Time separation between direct path and multipath
$\tau_d$	- Propagation time for direct path
$\tau_m$	- Propagation time for multipath
$\omega$	- Radian frequency
$\omega(t)$	- Instantaneous radian frequency



- $\Delta\omega_x$  - Deviation of carrier frequency associated with message signal
- $\Delta\omega_v$  - Deviation of carrier frequency associated with sweeping waveform
- $\omega_v$  - Sweeping frequency
- $\omega_n$  - Natural frequency of Phase-Locked Loop
- $\xi$  - Damping factor associated with Phase-Locked Loop
- $\sigma^2$  - Variance
- $\eta$  - Multipath suppression (%)
- $\phi$  - Angle separation between direct and multipath spectra



## CHAPTER I

### INTRODUCTION

Until recent years, landbased development of natural resources has met the demands for raw materials while offshore resource development, with the exception of the fishery has been ignored. The reason for this has been the extreme cost of the technologies necessary for extracting offshore raw materials such as oil and gas. The present fuel shortage and the resulting high costs of imported fuel, has made offshore oil and gas exploration feasible. This has triggered diverse research in the development of underwater technologies.

One of the essential needs for underwater operations is reliable and efficient communications. Remote control and telemetry for underwater equipment, diver voice communications and diverse oceanographic measurements are but a few examples where transmission of information is required.

#### 1.1 Underwater Communications and Acoustics

Man first learned to communicate underwater when he discovered that sound waves, produced by two rocks being struck, would travel long distances underwater.

Underwater communications was not to become important, however, until after the first world war when it was realized the role it could play from a military point of view. Research conducted since that time has mainly involved the

evaluation of electromagnetic and acoustic waves for underwater communication. More recently, communication by means of an electric current field (ECF) has been investigated [38]. The main drawback of ECF communication is its limited range. The received signal strength is inversely proportional to the water conductivity and the cube of the range separating transmitter and receiver.

The major limitation in the use of electromagnetic radiation for underwater communication is the severe absorption of electromagnetic waves by sea water. The signal attenuation in water as a function of wavelength is plotted in Figure 1.1a [15]. Except for the narrow band of optical frequencies, and only then in clear water, the attenuation is prohibitively high. This severe attenuation factor coupled with the problems associated with antennae design and bandwidth attainable, render communication using electromagnetic waves of limited application [2].

In comparison with electromagnetic wave propagation, the attenuation of acoustic energy by sea water is far less severe. A plot showing the attenuation of acoustic energy as a function of frequency is shown in Figure 1.1b [34]. It is due to this relatively low attenuation that an acoustic carrier has been extensively used for underwater communication.

Underwater acoustic communication is, however, affected by refraction, reverberation and noise, inherent to the underwater acoustic channel. Extensive research [14], [18], [20], [21], [34] has gone into these areas to

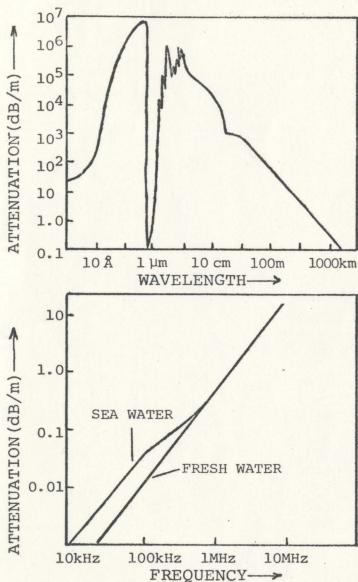


Figure 1.1a (above) The Attenuation of Electromagnetic Waves in Clear Sea Water

Figure 1.1b (below) The Attenuation of Sound in Sea and Fresh Water as a Function of Frequency

aid the designers of underwater acoustic communication systems. As a result, attenuation, refraction and noise can be accounted for with relative ease in the design. The major problem confronting designers is reverberation.

Reverberation is the result of two effects, scattering and multipath. Scattering results when the acoustic wave encounters various inhomogenities such as plankton, air bubbles and small fish. This causes random fluctuation of the signal along the transmission path. The second effect, multipath, is caused by the reflections of the acoustic wave at the surface or bottom boundaries. In certain situations, as indicated in Figure 1.2, a transmitted signal is received as a sum of the direct path and delayed multipath signals. This interaction severely affects communications [2], [9]. Since the intensity of multipath is proportional to the transmitted signal amplitude, increasing the transmitting power is an ineffective means of reducing multipath [24].

In this thesis, a novel concept is developed to reduce the multipath interference affecting underwater acoustic communication. The idea proposed is based on the observation that the time separation between direct and multipath waveforms can be utilized to suppress the multipath interference. Multipath suppression is achieved by employing unique modulation and demodulation schemes.

A computer evaluation was conducted to determine the improved performance of a system employing the multipath

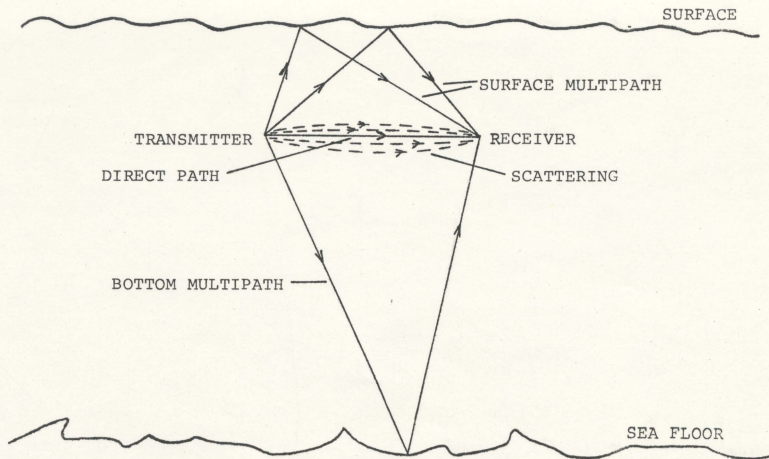


Figure 1.2 Underwater Acoustic Communication Link

suppression method. Favourable results warranted testing of an experimental system.

A system prototype was built and tested using the Multipath Channel Simulator developed. Successful tests conducted at sea during May 15-30, 1978 on board the Canadian Scientific Ship "Hudson", proved the receiver's ability to suppress multipath.



## CHAPTER II

### MODEL OF THE UNDERWATER ACOUSTIC COMMUNICATION CHANNEL

#### 2.1 Introduction

In this chapter a simplified mathematical and geometrical model for an underwater multipath channel communication system is proposed to aid in the development of the concept mentioned in Chapter I.

#### 2.2 Model Formulation

It is assumed that an acoustic link between transmitter and receiver as shown in Figure 1.2 is comprised of direct and multipath signals.

A complete underwater communication system can be represented by a block diagram shown in Figure 2.1. In the Transmitter, a baseband message signal  $x(t)$  has its spectrum translated in frequency by suitable modulation of a carrier signal. The electrical signal is then transformed into an acoustic signal  $s(t)$  by a transducer represented by the filter  $T_T(j\omega)$ . The signal  $s(t)$  propagates through the underwater channel and is transformed back into an electrical signal by a receiving transducer  $T_R(j\omega)$ . The received signal is applied to the system receiver, where the signal is demodulated and the transmitted message  $x'(t)$  is recovered.  $n(t)$  represents ambient noise [18] and will not be considered in this thesis.

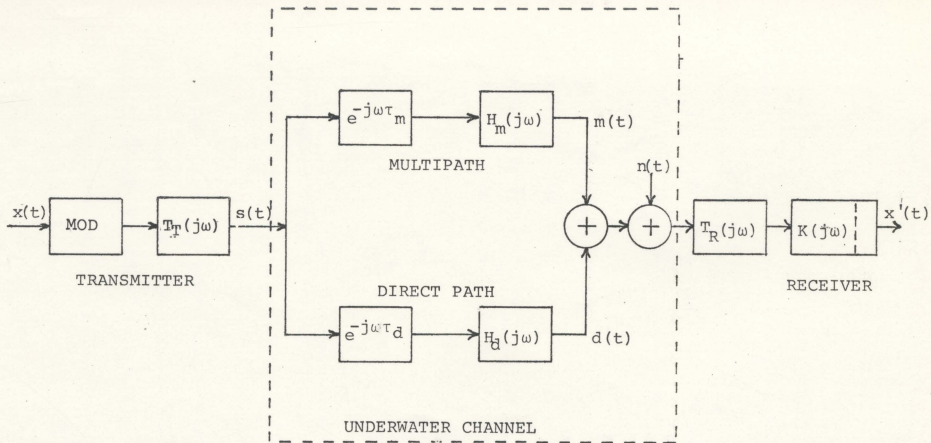


Figure 2.1 An Underwater Communication System Model

The underwater channel is considered as a parallel branch representing the direct and indirect path. The geometrical distance  $s$  separating the transmitter and receiver and the sound velocity  $c$  invoke a time delay  $\tau_d$  represented by filter  $e^{-j\omega\tau_d}$  in the direct path,

$$\tau_d = s/c \quad (2.1)$$

The filter  $H_d(j\omega)$  represents signal spreading and absorption by the medium. This filter is assumed to have a real transfer function.

$$H_d(j\omega) = H_d(\omega) \quad (2.2)$$

Based on empirical data [34] an expression is obtained which conservatively approximates  $H_d(\omega)$  by

$$H_d(2\pi f) = -[20 \log s + 36.4(10^{-5})fs] \text{dB} \quad (2.3)$$

for  $20\text{kHz} \leq f \leq 100 \text{ kHz}$

where  $s$  is the distance between transmitter and receiver in meters,

$f$  is the frequency of the transmitted signal in kHz,

$H_d(2\pi f)$  is expressed in dB referring to  $1\mu$  bar.

Clearly,  $H_d(\omega)$  is the transfer function of a low pass filter.

A time delay  $\tau_m$  in the indirect path of Figure 2.1 is related to the earliest multipath signal. It is assumed that under normal conditions<sup>1</sup>, the geometry of Figure 1.2 represents a typical acoustic link. Thus, multipath propagation time will be longer than the propagation time of the direct path, ie;

<sup>1</sup>Normal conditions ensure that the geometrical distance for multipath is greater than the direct path. Severe bending of the wave due to refraction may distort normal conditions such that multipath arrives before the direct path [21].

$$\tau_m > \tau_d \quad (2.4)$$

A filter  $H_m(j\omega)$  represents the combined effect of all multipath signals. It is basically a low pass filter due to similar considerations as for  $H_d(j\omega)$ . Longer distances for multipath imply, however, higher attenuation and therefore a smaller bandwidth of  $H_m(j\omega)$  compared to  $H_d(j\omega)$  is expected.

The random and time varying nature of multipath suggests that the modelling filter  $H_m(j\omega)$  should be a time variant, random filter described in probabilistic terms rather than the deterministic transfer function  $H_m(j\omega)$ .

With this approach, the time dependence can be explicitly indicated by writing

$$H_m(j\omega) = H_m(\omega, t) e^{j\psi_m(\omega, t)} \quad (2.5)$$

where  $H_m(\omega, t) = |H_m(j\omega)|$

and  $\psi_m(\omega, t) = \angle H_m(j\omega)$

whereas the random character of  $H_m(j\omega)$  can be introduced by considering  $H_m(\omega, t)$  and  $\psi_m(\omega, t)$  as random processes for any particular  $\omega$ .

A simplified probabilistic model for multipath [24], [29], assumes Rayleigh distribution for  $H_m(\omega, t)$  and uniform distribution for phase  $\psi_m(\omega, t)$ .

According to Figure 2.1, the received signal  $r(t)$  is a sum of direct and multipath waveforms.

### 2.3 Impulse Response of the Model

When a delta pulse is applied at the input of the underwater channel model, ie.  $s(t) = \delta(t)$ , the received signal  $r(t)$  will be as shown schematically in Figure 2.2. The direct path impulse response  $d(t)$  has a finite width due to the low-pass nature of the filter  $H_d(j\omega)$ . The multipath signal  $m(t)$  is the impulse response of the time varying random filter  $H_m(j\omega)$ . In effectively modelling multipath, information pertaining to its intensity and duration is required. In general, spherical spreading of the acoustic wave through the medium is assumed. This implies that the rate of decay of multipath is inversely proportional to the square of the time. A typical observed decay of multipath as found in [14] is shown in Figure 2.3. Because of the finite energy carried by the multipath,

$$\lim_{t \rightarrow \infty} E\{m^2(t)\} = 0 \quad (2.6)$$

where  $E\{\cdot\}$  denotes the expected value, the multipath duration time  $T$  indicated in Figure 2.2, can be arbitrarily defined as the time span for which  $E\{m^2(t)\}$  is significant with respect to the intensity of the direct path return. This relationship can be associated with the geometry of a situation, as suggested by Figure 2.4.

### 2.4 Response of the Model to a Harmonic Signal

Consider a harmonic signal (carrier) applied to the input of the underwater channel model



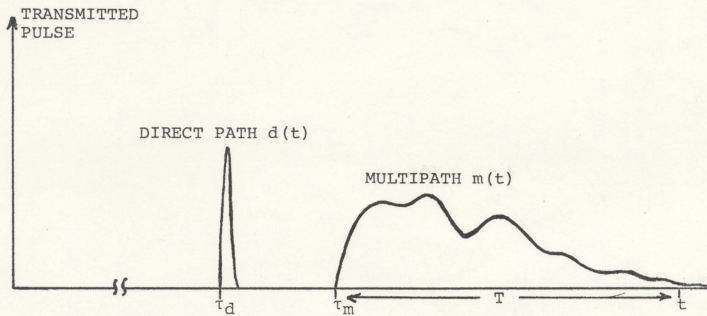


Figure 2.2 Impulse Response of the Channel Model



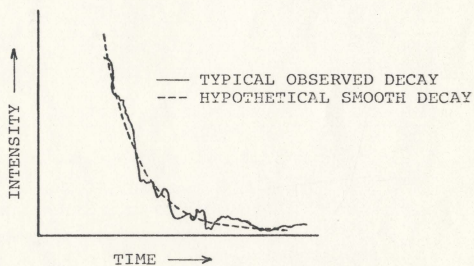
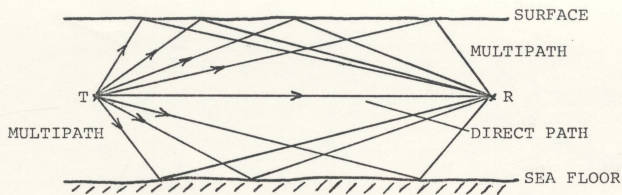
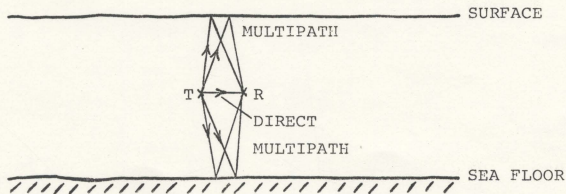
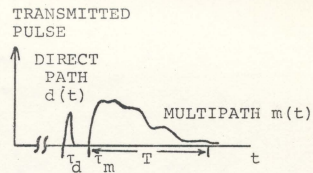


Figure 2.3 Decay of Reverberation Intensity



a) Long Range Shallow Water Communications



b) Short Range Deep Water Communications

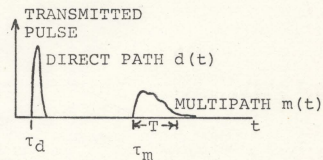


Figure 2.4 The Effect of Geometry on the Received Signal Structure

$$s(t) = A_C \cos \omega_C t = \operatorname{Re}\{A_C e^{j\omega_C t}\}; -\infty \leq t \leq \infty \quad (2.7)$$

The output of the model  $r(t)$  can be expressed by

$$\begin{aligned} r(t) &= \operatorname{Re}\{A_C e^{j\omega_C t} [e^{-j\omega_C \tau_m H_m(j\omega_C)} + e^{-j\omega_C \tau_d H_d(j\omega_C)}]\} \\ &= \operatorname{Re}\{I(t) e^{j(\omega_C t + \alpha(t))} + J e^{j(\omega_C t + \beta)}\} \end{aligned} \quad (2.8)$$

$$\text{where } I(t) = A_C H_m(\omega_C, t) \quad (2.8a)$$

$$\alpha(t) = -\omega_C \tau_m + \psi_m(\omega_C, t) \quad (2.8b)$$

$$J = A_C H_d(\omega_C) \quad (2.8c)$$

$$\beta = -\omega_C \tau_d \quad (2.8d)$$

In phasor notation,  $I(t)e^{j\alpha(t)}$  represents the time varying multipath signal  $m(t)$ , while phasor  $Je^{j\beta}$  represents the direct path signal  $d(t)$ . The geometrical sum of these two phasors as shown in Figure 2.5, results in  $R(t)e^{j\gamma(t)}$ , representing the composite received signal  $r(t)$

$$R(t)e^{j\gamma(t)} = I(t)e^{j\alpha(t)} + Je^{j\beta} \quad (2.9)$$

For constant values of  $J$  and  $\beta$ , the direct path signal  $d(t)$ , has only one frequency component, located at  $\omega_C$ . The multipath signal however, is both amplitude and angle modulated

$$m(t) = I(t) \cos[\omega_C t + \alpha(t)] \quad (2.10)$$

and occupies a finite frequency band. Because  $I(t)$  and  $\alpha(t)$  are in practice, slow varying functions of time, the frequency band occupied by  $m(t)$  is narrow and centered at  $\omega_C$ . As a result, the received signal  $r(t)$ , is also amplitude and frequency modulated

$$r(t) = R(t) \cos[\omega_C t + \gamma(t)] \quad (2.11)$$

The instantaneous frequency of the received signal is

$$\omega_C(t) = d\gamma(t)/dt + \omega_C \quad (2.12)$$

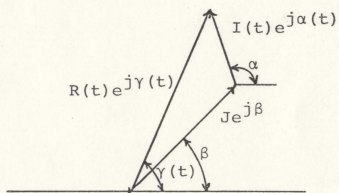


Figure 2.5 Phasor Representation for the Direct and Multipath Signals

The presence of interfering amplitude and angle modulation of the received carrier reflects difficulties encountered in underwater communications.

## CHAPTER III

### SWEPT CARRIER COMMUNICATIONS

#### 3.1 Introduction

The interfringing amplitude and angle modulation mentioned earlier, renders conventional modulation schemes susceptible to the effects of multipath [24]. Multipath is particularly severe in shallow water transmission, where strong surface and bottom reflections are encountered. No clearly advantageous modulation scheme has been found, though a number of different systems have been proposed and tested [3], [24], [25].

Time, frequency and space diversity are typical techniques employed in reducing multipath interference [24]. In general, such techniques tend to be restrictive with respect to transmission speed achievable, required system complexity and resulting high cost.

The concept of swept carrier communications, described in this chapter, refers to a transmission scheme which could be considered as a simultaneous time and frequency diversity technique. The suggested implementation results in a relatively simple system.

#### 3.2 Swept Carrier Communications

In describing the Swept Carrier Communication Concept, a situation is considered in which the carrier of (2.7) is transmitted through the channel model of Figure 2.1.



It is assumed that the transmitting and receiving transducer characteristics  $T_T(j\omega)$ ,  $T_R(j\omega)$  are constant over a broad frequency range, i.e.

$$T_T(j\omega) = T_R(j\omega) = 1 \quad \text{for } \omega_{\min} \leq \omega \leq \omega_{\max} \quad (3.1)$$

The receiver's front filter  $K(j\omega)$  is assumed to have a band pass frequency characteristic, centered at the carrier frequency  $\omega_c$ , bandwidth  $B_r$  and impulse response duration time,  $b$ .

In sequel, an instantaneous and possibly time varying spectrum  $F(\omega, t)$  is introduced for a signal in time window  $b$ .

In particular, the instantaneous spectra of the direct path signal  $d(t)$  and multipath signal  $m(t)$  are denoted by  $F_d(\omega, t)$  and  $F_m(\omega, t)$  respectively.

For a sufficiently high carrier frequency, i.e.,

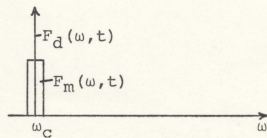
$$2\pi/\omega_c \ll b \quad (3.2)$$

the instantaneous spectra  $F_d(\omega, t)$  and  $F_m(\omega, t)$  are narrow-band and essentially time independent as shown schematically in Figure 3.1a, where  $F_d(\omega, t)$  is approximately a single frequency component located at  $\omega_c$ .

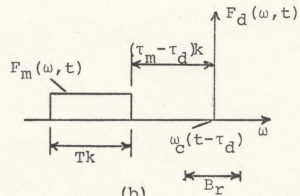
Suppose now the carrier frequency  $\omega_c$  is changing linearly in time, i.e.,

$$\omega_c(t) = kt \quad (3.3)$$

where  $k$  is a proportionality constant. The change in carrier frequency is followed by changes of the instantaneous spectra  $F_d(\omega, t)$  and  $F_m(\omega, t)$ . If the rate of change is slow enough,  $F_d(\omega, t)$  will remain approximately a single frequency component located at  $\omega_c(t - \tau_0)$ . The spectrum  $F_m(\omega, t)$ , how-



(a)



(b)

Figure 3.1 Instantaneous Spectra of the Direct and Multipath Signals

ever, due to the time delay  $\tau_m > \tau_d$  is lagging  $F_d(\omega, t)$  and due to multipath duration  $T$ , is broadened proportionally to  $T$  as shown in Figure 3.1b. Clearly, if the receiver's band-pass filter with bandwidth  $B_r$  could track a slow change in  $\omega_c(t)$ , then the multipath signal spectrum would fall outside the filter bandwidth resulting, in principle, in a complete rejection of the multipath signal.

Narrowband modulation of the carrier by a message signal would broaden both  $F_d(\omega, t)$  and  $F_m(\omega, t)$  spectra, but with proper choice of system parameters, the frequency separation between  $F_d(\omega, t)$  and  $F_m(\omega, t)$  could be maintained.

The main practical problem in the implementation of this idea arises from the limited frequency range over which the carrier frequency can be swept. Water attenuation and transducer characteristics confine the sweeping range to a certain limit (3.1).

$$\omega_{\min} \leq \omega_c(t) \leq \omega_{\max} \quad (3.4)$$

For continuous operation therefore,  $\omega_c(t)$  has to be a periodic function of time  $f(t)$ . Since  $f(t)$  can always be represented by a Fourier Series, attention is limited to the harmonic sweeping waveform

$$v(t) = A_v \cos \omega_v t \quad (3.5)$$

to produce the continuous sweep of the carrier frequency

$$f(t) = \omega_c(t) = \omega_o + \Delta\omega_v \cos \omega_v(t) \quad (3.6)$$

where

$\omega_o$  - central frequency

$\omega_v = 2\pi/T_v$  - low sweeping frequency

$\omega_o - \Delta\omega_v = \omega_{\min}$  - minimum carrier frequency

$\omega_o + \Delta\omega_v = \omega_{\max}$  - maximum carrier frequency

The time-frequency relationship for the instantaneous spectra  $F_d(\omega, t)$  and  $F_m(\omega, t)$  is now more complex than that shown previously in Figure 3.1 for the linear sweep. To show this relationship, it is convenient to write the departure of the instantaneous carrier frequency from the central frequency  $\omega_o$ , as

$$\omega_c(t) - \omega_o = \Delta\omega_v \cos\omega_v t = \text{Re}\{\Delta\omega_v e^{j\omega_v t}\} \quad (3.7)$$

The projection of the rotating phasor  $\Delta\omega_v e^{j\omega_v t}$ , onto the real axis, indicates the transmitted carrier instantaneous frequency  $\omega_c(t)$ .

Similarly, the instantaneous frequency location of the direct path signal is given by

$$\text{Re}\{\Delta\omega_v e^{j\omega_v(t-\tau_d)}\} \quad (3.8)$$

The instantaneous frequencies of the earliest and latest multipath signals are represented by phasors

$$\Delta\omega_v e^{j\omega_v(t-\tau_m)} \quad (3.9)$$

and

$$\Delta\omega_v e^{j\omega_v(t-\tau_m-T)} \quad (3.10)$$

respectively. The location of the instantaneous spectrum of the multipath signal  $F_m(\omega, t)$  lies between the projections of the above phasors, as shown in Figure 3.2a.

The multipath spectrum  $F_m(\omega, t)$  changes both its position and width  $M$  as a periodic function of time. Assuming the time origin at  $\tau_d$ , a more convenient geometrical model is obtained for finding the locations of  $F_d(\omega, t)$  and  $F_m(\omega, t)$  and is shown in Figure 3.2b. The multipath spectrum, width and location are obtained as the projection of

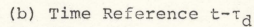
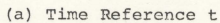


Figure 3.2 Phasor Representation of the Swept Carrier Concept for  $F_d(\omega, t)$  and  $F_m(\omega, t)$

arc a which is rigidly attached to the rotating phasor

$$\Delta\omega_v e^{j\omega_v(t-\tau-T/2)} \quad (3.11)$$

where

$$\tau = \tau_m - \tau_d \quad (3.12)$$

From geometrical consideration, the multipath spectrum central frequency  $\omega_m(t)$  is given by

$$\omega_m(t) = \omega_o + \Delta\omega_v \cos(\omega_v t - \omega_v \tau - \omega_v T/2) \quad (3.13)$$

It is assumed that the receiver's tracking filter of bandwidth  $B_r$  follows the instantaneous frequency  $\omega_c(t)$  of the direct path signal. As seen from figure 3.2b, the direct and multipath signal spectra move along the frequency axis periodically in time. Direct and multipath spectra separation is directly related to the angle  $\phi$  between phasor (3.11) and phasor

$$\Delta\omega_v e^{j\omega_v t} \quad (3.14)$$

The angle  $\phi$  is expressed as

$$\phi = \omega_c \tau + \frac{\omega_v T}{2} \quad (3.15)$$

Multipath signal suppression results from the following mechanisms:

- (1) For situations when  $M$  is smaller than the carrier sweep range  $2\Delta\omega_v$ , there exist periods of time when the tracking filter bandwidth  $B_r$  and the multipath spectra,  $F_m(\omega, t)$  do not overlap. When  $F_m(\omega, t)$  falls outside the receiving filter bandwidth, rejection of  $F_m(\omega, t)$  by the receiver results.



For such situations, the maximum direct and multipath spectra separation resulting in maximum multipath suppression occurs when  $\phi$  in (3.15) equals  $\pi(180^\circ)$ , i.e.,

$$\phi = \omega_V \tau + \frac{\omega_V T}{2} = \pi \quad (3.16)$$

- (2) For situations when the tracking filter bandwidth and the multipath spectra overlap, multipath suppression is still possible, if

$$M > B_r \quad (3.17)$$

For such situations, only a portion of the multipath energy falls within the receiving filter bandwidth at any particular time.

Any narrowband modulation of the swept carrier by a message signal, will not appreciably alter the geometrical model shown in Figure 3.2b. When modulation is applied, the instantaneous spectrum of the direct signal will occupy a finite frequency band, and the multipath spectrum will be broader than that without modulation.

With the aid of the geometrical model of Figure 3.2b, one can expect a direct relationship between the receiver's ability to suppress multipath and the ratio of the swept carrier range  $2\Delta\omega_V$  to the receiver's tracking filter bandwidth  $B_r$ . The maximum value of this ratio is, however, constrained by assumptions made earlier.

## CHAPTER IV

### COMPUTER EVALUATION OF THE SWEPT CARRIER SYSTEM PERFORMANCE

#### 4.1 Introduction

In this chapter detailed consideration is given to the performance of the swept carrier system discussed qualitatively in Chapter III.

For the convenience of exposition, the multipath spectrum located between the projections of phasors (3.9) and (3.10) as shown in Figure 3.2b, is assumed to have a band pass noise characteristic. The total input multipath power (noise power) for any given time  $t$  is assumed to be constant and equal to one, i.e.,

$$\int_{-\infty}^{\infty} F_m(\omega, t) d\omega = 1, \text{ for all } t \quad (4.1)$$

Assuming constant power of the direct path signal within the tracking filter bandwidth, it is apparent that the multipath power within the filter bandwidth will determine signal to noise ratio and therefore system performance.

Due to the rather complex interaction between tracking filter and the time varying multipath spectrum, the system performance was evaluated through computer simulation.

The tracking filter assumed for simulation has real characteristics, i.e.,

$$k(j\omega) = k(\omega, t) = \frac{1}{[1 + [(\omega_0 - \omega_C(t) / (B_T/2)]^4]^{1/2}} \quad (4.2)$$

where  $\omega_0$  is the central carrier frequency

$\omega_c(t)$  is the instantaneous carrier frequency

$B_r/2$  is the one sided 3dB filter bandwidth

The instantaneous noise power  $p(t)$  at the output of the tracking filter  $k(\omega, t)$  is expressed as

$$p(t) = \int_M F_m(\omega, t) |k(\omega, t)|^2 d\omega \quad (4.3)$$

The value of  $p(t)$  varies as a periodic function of time with period  $T_v$  equal to that of the sweeping signal  $v(t)$ .

The average noise power  $P$  at the output of the tracking filter is given by

$$P = \frac{1}{T_v} \int_0^{T_v} p(t) dt \quad (4.4)$$

The parameters which directly affect the value of  $P$  are

- (1)  $\phi$  - angle separation between direct and multipath spectra
- (2)  $\omega_v T$  - angular separation between phasors (3.9) and (3.10) which determine multipath spectrum width  $M$ .
- (3)  $2\Delta\omega_v/B_r$  - ratio of the carrier sweep range to the receiver's tracking filter bandwidth.

The evaluation of system performance follows, based on the average output multipath power  $P$  as a function of the above parameters.

## 4.2 Computer Simulation Results

The angle separation  $\phi$  between direct and multipath spectra is expressed in (3.15) as

$$\phi = \omega_v T + \frac{\omega_v T}{2}$$

Figure 4.1 shows  $p(t)$  and  $P$  plotted over one complete cycle of  $v(t)$  for different values of  $\phi$ .

The results of Figure 4.1, including the instantaneous power variation  $\sigma_p^2(t)$

$$\sigma_p^2(t) = \frac{1}{T_v} \int_0^{T_v} (P - p(t))^2 dt \quad (4.5)$$

about the average noise power and multipath suppression  $\eta$

$$\eta = (1 - P) 100\% \quad (4.6)$$

are summarized in Table 4.1.

For  $\phi = 0^\circ$  / (i.e. zero sweeping frequency) frequency separation between direct and multipath spectra is not possible. System performance resembles conventional transmission where the receiver is subjected to maximum multipath interference. For  $\phi = 180^\circ$ , multipath suppression is optimum with respect to lowest average output noise power  $P$ . For the case of  $\phi = 360^\circ$ , the multipath spectrum is broadened such that significant "escape" of the tracking filter from multipath is not possible. Multipath suppression is still achieved as a result of the second mechanism discussed in Chapter 3. In the latter case, the noise power variation  $p(t)$  due to multipath is minimum. This can be considered as advantageous in applications where large fluctuation in noise power cannot be tolerated.

$\omega_v T$ , as seen in Figure 3.2 represents the angular separation between earliest and latest multipath signals and defines multipath spectrum width  $M$ . The average power  $P$

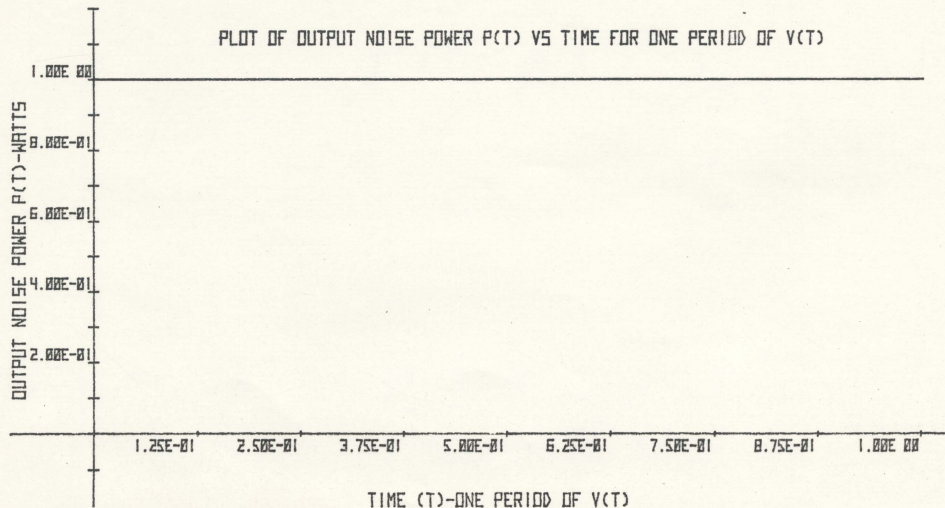


Figure 4.1a  $p(t)$  vs time for one period of  $v(t)$  for  $\phi=0^\circ$

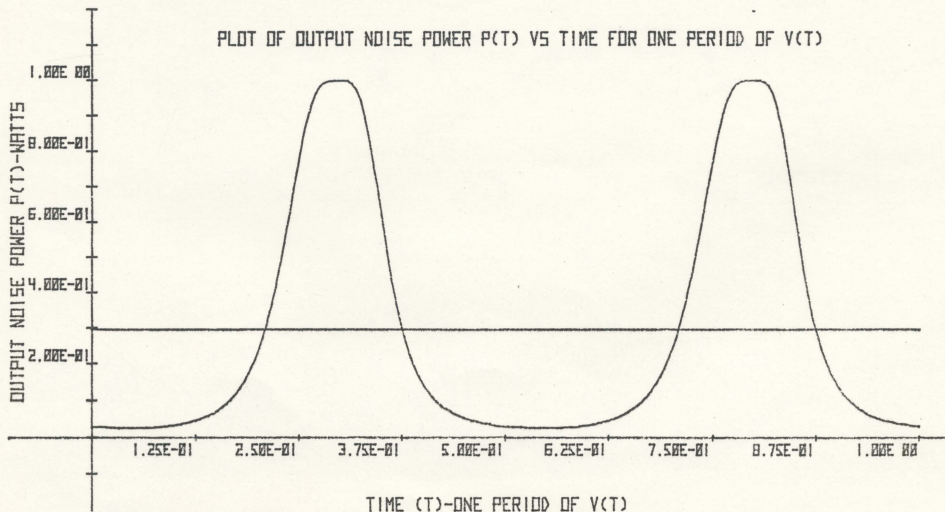


Figure 4.1b  $p(t)$  vs time for one period of  $v(t)$  for  $\phi=30^\circ$



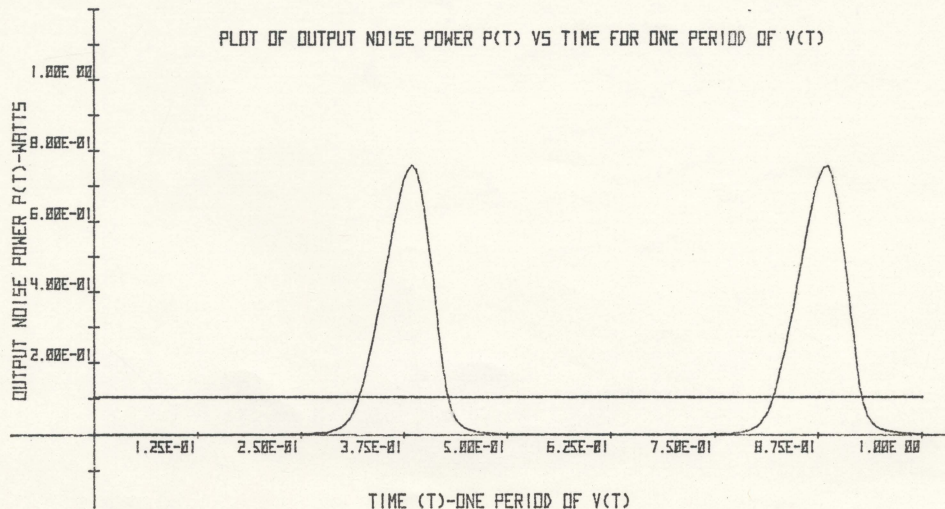


Figure 4.1c  $p(t)$  vs time for one period of  $v(t)$  for  $\phi = 90^\circ$

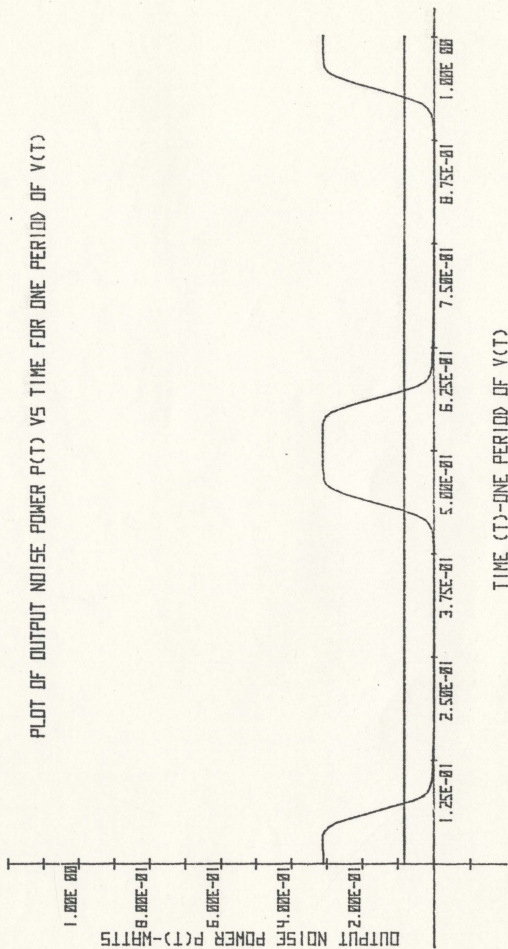


Figure 4.1d  $p(t)$  vs time for one period of  $v(t)$  for  $\phi = 180^\circ$

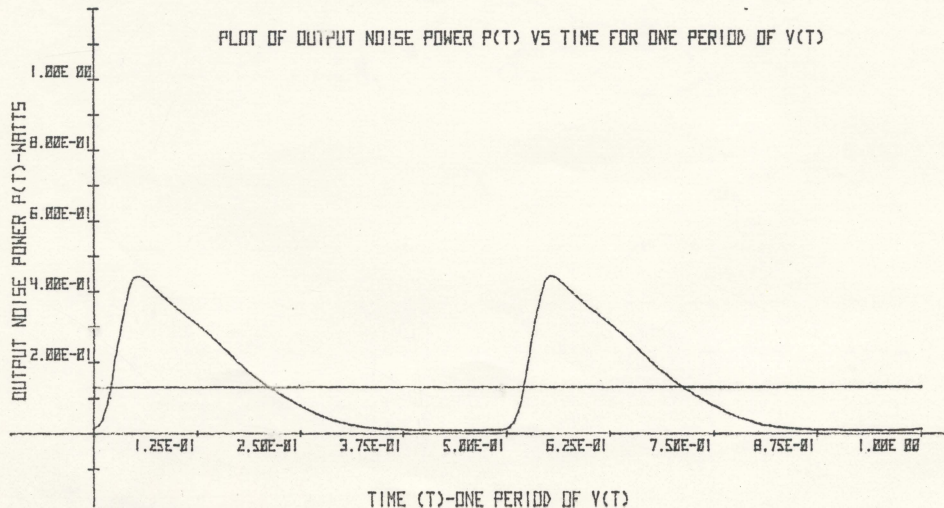


Figure 4.1e  $p(t)$  vs time for one period of  $v(t)$  for  $\phi=270^\circ$

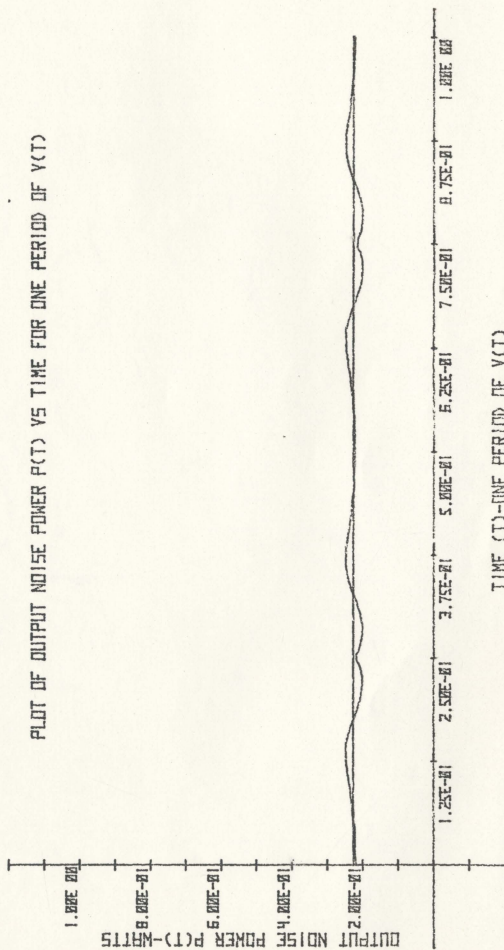


Figure 4.1f  $p(t)$  vs time for one period of  $v(t)$  for  $\phi=360^\circ$

TABLE 4.1 Computer Simulation Results showing the Dependence of P on

Delay time  $\tau$  separating direct path and multipath - 0.015 secs

Multipath duration time T - 0.01 secs

Carrier sweep range  $2\Delta\omega_v$  - 30,000 ( $2\pi$ ) rad/sec

Receiver's tracking filter bandwidth  $B_r$  - 6000 ( $2\pi$ ) rad/sec

Figure	$\omega_v(2\pi)$ Hz	$\phi$ Deg.	$\omega_v T$ Deg.	P	$\sigma_p^2(t)$	$\eta$	Remarks
4.1a	$\approx 0$	$\approx 0$	$\approx 0$	1	$\approx 0$	$\approx 0\%$	Conventional Transmission
b	4.2	30	15	$2.98(10^{-1})$	$1.21(10^{-1})$	70.2%	
c	12.5	90	45	$1.05(10^{-1})$	$4.50(10^{-2})$	89.5%	
d	25.0	180	90	$8.24(10^{-2})$	$1.58(10^{-2})$	91.8%	Maximum Suppression
e	37.5	270	135	$1.33(10^{-1})$	$2.04(10^{-2})$	86.7%	
f	50.0	360	180	$2.27(10^{-1})$	$2.16(10^{-4})$	77.3%	Minimum Variance

vs  $\omega_V$  with  $\omega_V T$  as a parameter is shown in Figure 4.2.

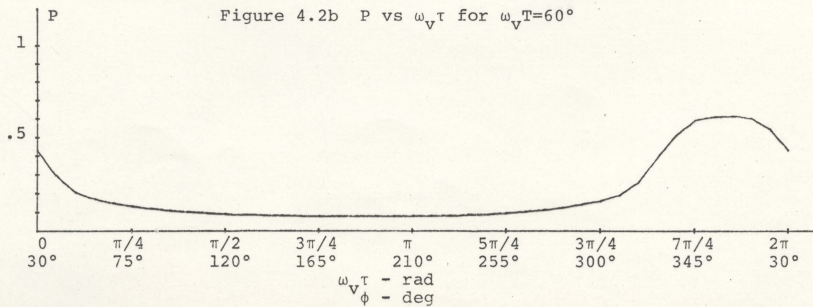
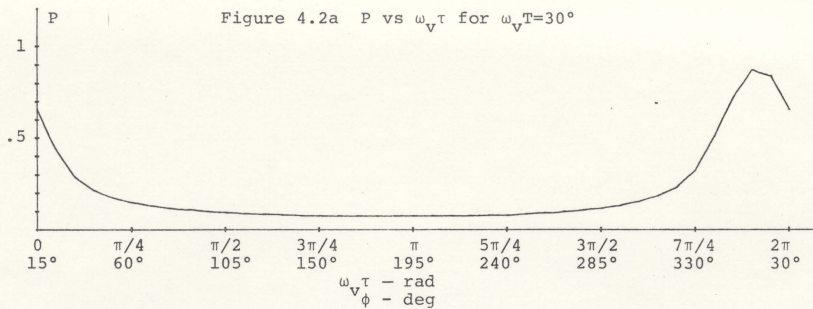
The results obtained and summarized in Table 4.2, provide important information about system sensitivity with respect to the sweeping frequency for various multipath conditions. For large values of  $\omega_V T$ , the system is less sensitive (as indicated by the variance of  $P$ ) with respect to  $\omega_V$ .

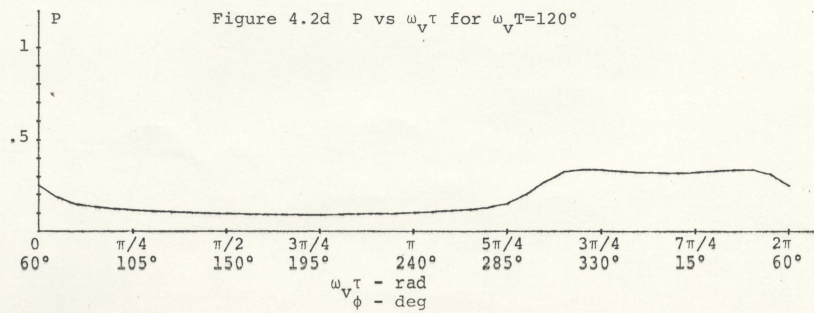
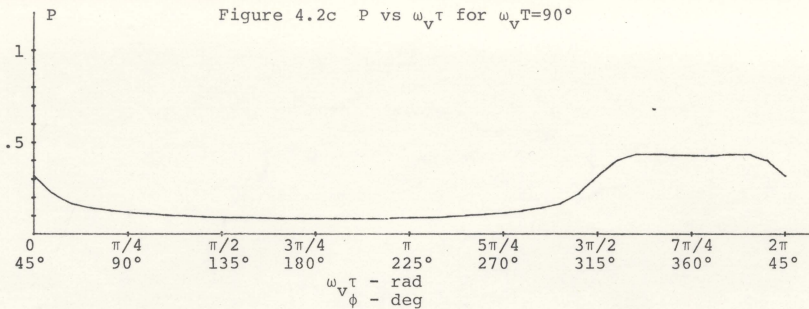
Figure 4.3 shows a dependence between the average output noise power and the ratio of the carrier sweep range to the receiver's tracking filter bandwidth. The dependence is shown for  $\omega_V T = 30^\circ$  and  $\omega_V T = 360^\circ$  for  $\phi = 180^\circ$ . The results, summarized in Table 4.3 supports previous reasoning that an increase in ratio  $2\Delta\omega_V/B_r$  improves system performance.

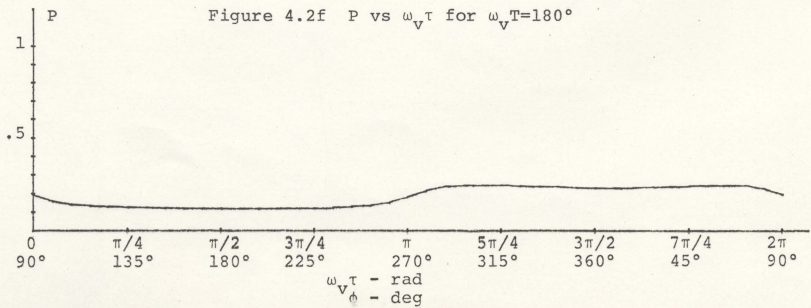
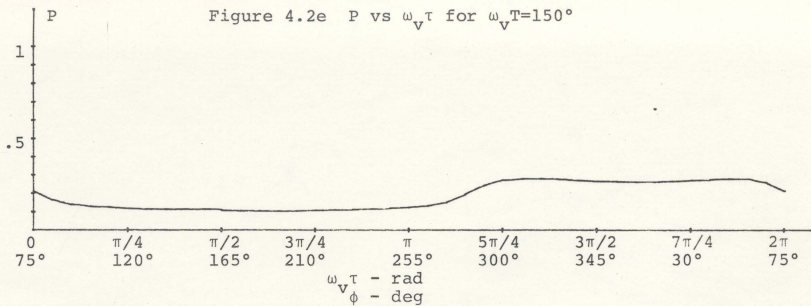
Physical interpretation of the two cases considered are now given. Values of  $\omega_V T$  equal to  $30^\circ$  and  $360^\circ$  identify with short range deep water communications and long range shallow water communications respectively (Figure 2.4). Since  $T$  is the dominating parameter for long range shallow water communications, an optimum sweep governed by (3.16) will result in a broad multipath spectrum. The results of Table 4.3 indicate  $P$  decreasing faster for  $\omega_V T = 30^\circ$  than for  $\omega_V T = 360^\circ$ . This result is expected due to the mechanisms outlined in Chapter III.

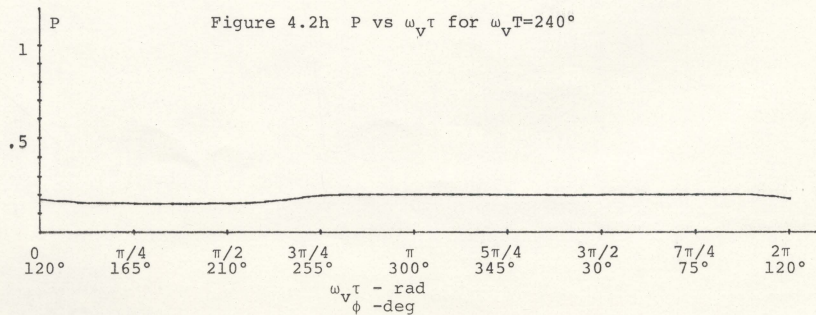
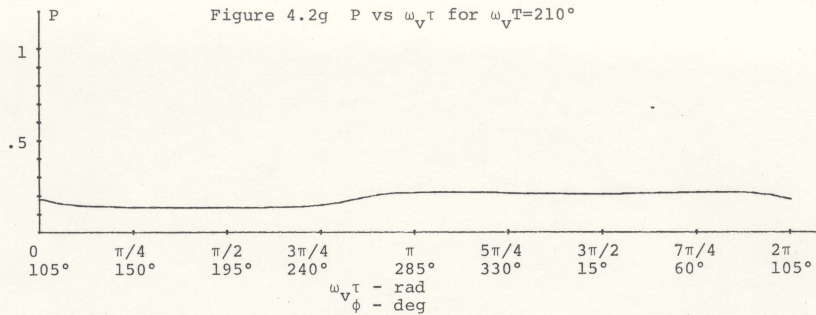
The simulation conducted and detailed in this chapter was performed using the HP-9825 computer. A listing of the program used is included in Appendix A.

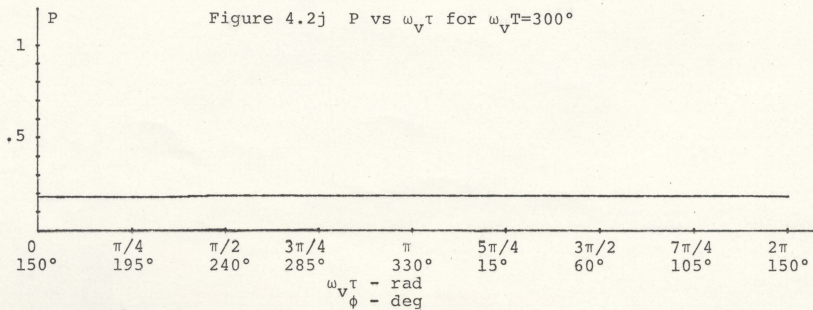
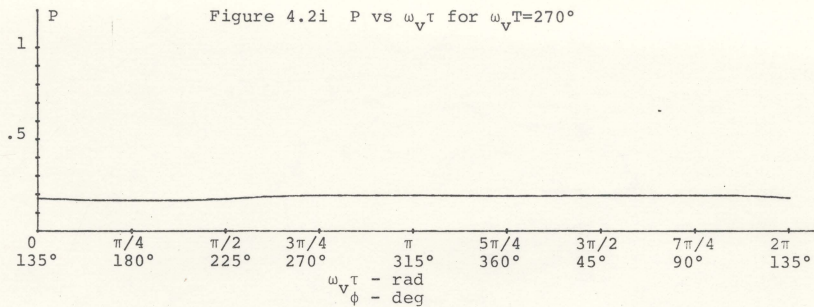












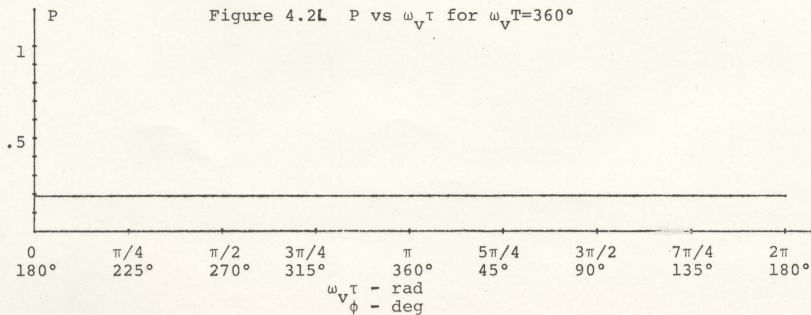
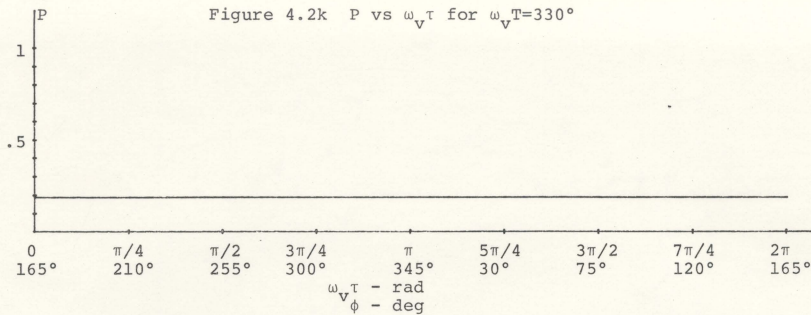





TABLE 4.2 Computer Simulation Results showing the Dependence of P on  $\omega_v T$

Carrier sweep range  $2\Delta\omega_v - 30,000(2\pi)\text{rad/sec}$

Receiver's tracking filter bandwidth  $B_r - 6000(2\pi)\text{rad/sec}$

Figure	$\omega_v T$ deg.	max P	min P	$\sigma_P$	Remarks
4.2a	30	$8.71(10^{-1})$	$7.42(10^{-2})$	$4.96(10^{-2})$	narrow multi- path spectrum  
b	60	$6.12(10^{-1})$	$7.72(10^{-2})$	$3.19(10^{-2})$	
c	90	$4.34(10^{-1})$	$8.24(10^{-2})$	$1.83(10^{-2})$	
d	120	$3.40(10^{-1})$	$9.13(10^{-2})$	$1.00(10^{-2})$	
e	150	$2.81(10^{-1})$	$1.04(10^{-1})$	$5.36(10^{-3})$	
f	180	$2.45(10^{-1})$	$1.17(10^{-1})$	$2.85(10^{-3})$	
g	210	$2.18(10^{-1})$	$1.34(10^{-1})$	$1.21(10^{-3})$	
h	240	$2.02(10^{-1})$	$1.51(10^{-1})$	$4.28(10^{-4})$	
i	270	$1.94(10^{-1})$	$1.67(10^{-1})$	$9.81(10^{-5})$	
j	300	$1.89(10^{-1})$	$1.80(10^{-1})$	$9.58(10^{-6})$	
k	330	$1.88(10^{-1})$	$1.86(10^{-1})$	$2.01(10^{-7})$	
l	360	$1.87(10^{-1})$	$1.87(10^{-1})$	0	broad multi- path spectrum

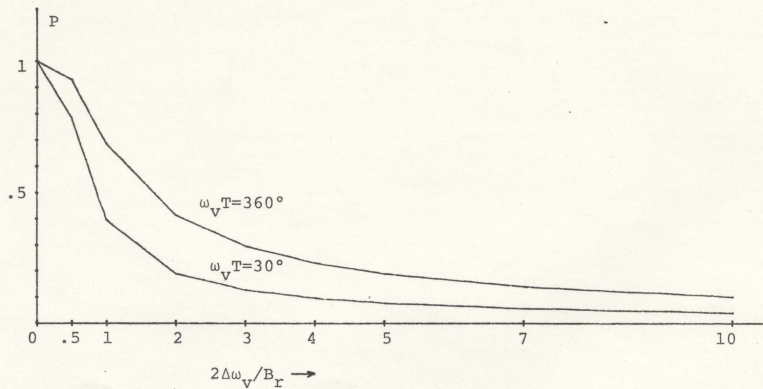


Figure 4.3  $P$  vs  $2\Delta\omega_V/B_r$  for  $\omega_V T = 30^\circ$  and  $\omega_V T = 360^\circ$  for  $\phi = 180^\circ$

TABLE 4.3 Computer Simulation Results showing the Dependence of P on  $2\Delta\omega_V/B_r$

Receiver's tracking filter bandwidth  $B_r = 6000(2\pi)\text{rad/sec}$   
Lagging angle  $\phi = 180^\circ$

$2\Delta\omega_V/B_r$	$\omega_V T = 30^\circ$		$\omega_V T = 360^\circ$	
	P	$\eta$	P	$\eta$
0	1	0%	1	0%
.5	$7.85(10^{-1})$	22.0%	$9.29(10^{-1})$	7.1%
1	$3.98(10^{-1})$	60.2%	$6.86(10^{-1})$	31.4%
2	$1.89(10^{-1})$	81.1%	$4.14(10^{-1})$	58.6%
3	$1.26(10^{-1})$	87.4%	$2.95(10^{-1})$	70.5%
4	$9.45(10^{-2})$	90.5%	$2.28(10^{-1})$	77.2%
5	$7.58(10^{-2})$	92.4%	$1.87(10^{-1})$	81.3%
7	$5.42(10^{-2})$	94.6%	$1.37(10^{-1})$	86.3%
10	$3.80(10^{-2})$	96.2%	$9.91(10^{-2})$	90.1%

Remarks:

Average output noise power P decreases faster for  $\omega_V T = 30^\circ$  than for  $\omega_V T = 360^\circ$  due to mechanism 1 of Chapter III.

## CHAPTER V

### SWEPT CARRIER SYSTEMS

#### 5.1 Introduction

The swept carrier communication concept is applicable to any narrowband modulation applied for message transmission. The modulation scheme chosen will determine the implementation of the system prototype. The most obvious and simple choice would be either narrowband amplitude or frequency modulation.

#### 5.2 Functional Structure of a Swept Carrier System

Figure 5.1 represents a possible functional structure for a swept carrier system. The low frequency harmonic signal  $v(t)$  sweeps the instantaneous carrier frequency  $\omega_c(t)$ , produced by the voltage controlled oscillator (VCO) over a desired frequency range,  $\omega_{\min}$  to  $\omega_{\max}$  where  $\omega_o$  is the central carrier frequency. The sweeping rate is determined by the sweeping signal frequency  $\omega_v$ .

Narrowband modulation of the carrier by a message signal  $x(t)$  is represented by the functional block MOD. The output signal is then transformed into an acoustic signal by  $T_T(j\omega)$ .

At the receiver, the sweeping signal  $v'(t)$  is recovered in the instantaneous carrier frequency recovery block IC.  $v'(t)$  is used to tune the central frequency of a tracking bandpass filter BPF, with bandwidth  $B_r$ . Demodu-

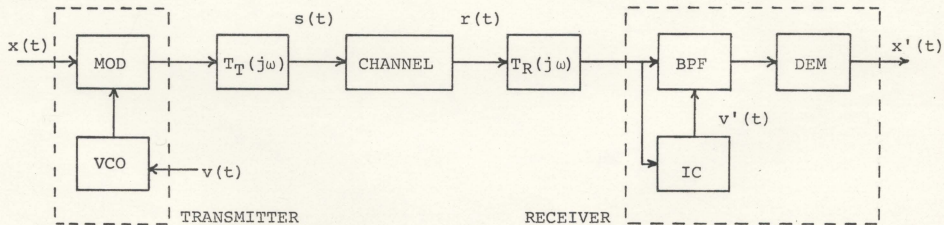


Figure 5.1 The Functional Structure of the Swept Carrier System

lation of the output signal of the bandpass filter is represented by DEM. The output from this demodulator is the received message signal  $x'(t)$ .

Particular implementation of MOD and DEM depends on the modulation scheme employed.

### 5.3 Swept Carrier Amplitude Modulation

When narrowband amplitude modulation is employed for message transmission, the transmitted signal  $s(t)$ , indicated in Figure 3.1, can be expressed in the normalized form by

$$s(t) = [1 + mx(t)] \cos[\omega_0 t + \Delta\omega_v \int_{-\infty}^t \cos \omega_v \lambda \, d\lambda] \quad (5.1)$$

where  $m$ , the modulation index, is less than 1, and the message signal  $x(t)$  is normalized such that  $|x(t)| \leq 1$ .

The instantaneous carrier frequency is

$$\omega_c(t) = \omega_0 + \Delta\omega_v \cos \omega_v t \quad (5.2)$$

and the direct path received signal envelope is given by:

$$e(t) = [A + mx(t)] H_d(j\omega_c(t)) |T(j\omega_c(t))| \quad (5.3)$$

where

$$T(j\omega) = T_T(j\omega) T_R(j\omega) \quad (5.4)$$

As shown in equation 5.3, the received direct path signal envelope is multiplicatively distorted due to non-uniform frequency response of the transducers<sup>1</sup> and the frequency dependent water attenuation reflected by  $H_d(j\omega_c(t))$ . This distortion is a slow varying, periodic function of time with period  $T_v$ . If the allowable minimum message sig-

<sup>1</sup>In chapter II,  $T(j\omega)$  was set equal to unity for the purpose of model development.



nal frequency is limited, an appropriate automatic gain control circuit can be used to remove this distortion without affecting envelope variation caused by a message signal.

### 5.3 Swept Carrier Frequency Modulation

For swept carrier frequency modulation, the transmitted signal  $s(t)$ , can be expressed in normalized form as

$$s(t) = \cos \left[ \omega_0 t + \Delta \omega_v \int_{-\infty}^t \cos \omega_v \lambda d\lambda + \Delta \omega_x \int_{-\infty}^t x(\lambda) d\lambda \right] \quad (5.5)$$

where  $\Delta \omega_x$  is the frequency deviation of  $\omega_c(t)$  associated with the message signal  $x(t)$ . The signal  $s(t)$  in (5.5) expresses double frequency modulation; broadband FM for the low frequency sweeping signal  $v(t)$  and narrowband FM for the message signal  $x(t)$ . When the direct path signal  $s(t)$ , is applied at the input of an ideal frequency demodulator, the output can be expressed by

$$e(t) = x(t) + x_i(t) + v'(t) \quad (5.6)$$

where  $x_i(t)$  is an additive periodical distortion with period  $T_v$ , caused by the non-linear phase characteristic of the transducers

$$x_i(t) = \frac{d}{dt} \angle T(j\omega_c(t)) \quad (5.7)$$

By limiting the allowable minimum message frequency, the message signal  $x(t)$ , can be separated by an appropriate high pass filter from the low frequency signals  $x_i(t)$  and  $v'(t)$ .

## CHAPTER VI

### PROTOTYPE IMPLEMENTATION AND TESTS

#### 6.1 Introduction

Narrowband frequency modulation has been chosen as the message modulation scheme in a swept carrier system prototype. Receiver implementation is particularly simple when a Phase-Locked Loop is used to perform simultaneously as a tracking filter and frequency demodulator [5], [13].

The functional block diagram of a Phase-Locked Loop (PLL) is shown in Figure 6.1. The phase of the incoming signal  $y_i$  is compared with the phase of a signal  $y_o$  produced by a voltage controlled oscillator (VCO). The phase difference between these two signals, after low pass filtering by the loop filter,  $F(s)$ , is applied to the VCO input. The loop is said to be in lock (see [5] for details) when the phase of the VCO signal tracks the phase of the input signal. The output of the loop filter is proportional to the instantaneous frequency of the input signal  $y_i$ . A Phase-Locked Loop can be characterized by its tracking range, defined as the frequency range over which lock can be maintained and a smaller capture range, defined as the frequency range over which lock can be acquired. In operation, the PLL approximates the behaviour of a bandpass tracking filter with bandwidth determined by the loop filter (as to be demonstrated) followed by a frequency demodulator [23]. The design details of the experimental system

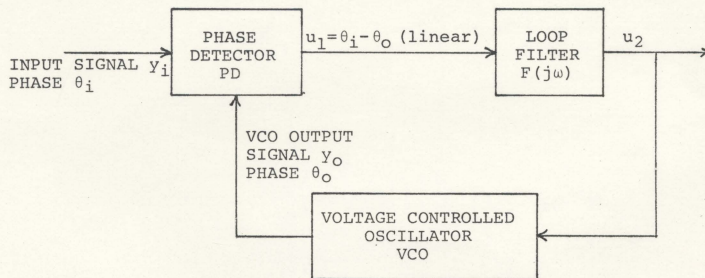


Figure 6.1 Functional Block Diagram of a Phased-Locked Loop

receiver are included in Appendix B.

The experimental system designed has the following parameters:

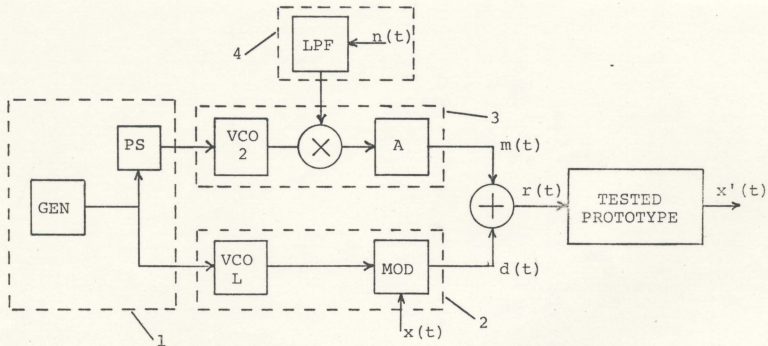
- central carrier frequency,  $f_o$  : 80kHz
- carrier sweep range,  $f_{\min}$  to  $f_{\max}$  : 65kHz to 95kHz
- sweeping frequency,  $f_v$  :  $f_v \leq 80\text{Hz}$
- message signal frequency,  $f_x$  :  $300\text{Hz} \leq f_x \leq 2\text{kHz}$
- carrier deviation caused by message signal,  $\Delta f_x$  :  $\pm 1\text{kHz}$
- receiving filter bandwidth,  $B_r$  : 6000 Hz

## 6.2 Swept Carrier Multipath Channel Simulator

Extensive laboratory testing of the prototype has been performed using the Swept Carrier Multipath Channel Simulator developed to provide controlled multipath conditions.

The Multipath Channel Simulator, shown in Figure 6.2a, follows in principle geometrical model discussed in Chapter II. The lower branch simulates the direct path signal  $d(t)$ . The harmonic sweeping waveform  $v(t)$  of frequency  $\omega_v$  is produced by generator GEN. This signal is used to vary the instantaneous frequency of the voltage controlled oscillator VCO1. The output signal of VCO1 is narrowband modulated by a message signal  $x(t)$  in the modulator, MOD. The resultant direct path signal has a time varying spectrum  $F_d(\omega, t)$  as indicated in Figure 3.2.

The upper branch of Figure 6.2a simulates the multipath signal  $m(t)$ . The lagging angle  $\phi$  is simulated by a con-



- 1 Feedback TWG500 Variable Phase Generator
- 2 HP 3312A FUNCTION GENERATOR
- 3 HP 3312A FUNCTION GENERATOR
- 4 HP 3722A NOISE GENERATOR

Figure 6.2a The Swept Carrier Multipath Channel Simulator



trolled phase shifted output of GEN. The band limited white noise at the output of the low pass filter LPF, is used to simulate the multipath signal  $m(t)$ . Multipath signal power is controlled by attenuator A. Finally, the sum of direct and multipath signals  $r(t)$  is used for testing the system receiver. The lab set-up is shown in Figure 6.2b.

A slight discrepancy does exist between the geometrical model of Figure 3.2 and the Swept Carrier Multipath Channel Simulator. The spectrum width  $M$  of the simulator remains constant in time, differing from that of the model in which  $M$  is varying in time. This discrepancy however seems to be acceptable for the purpose of the tests conducted.

### 6.3 Laboratory Tests

Initial tests in assessing system performance, involved an harmonic interfering signal added to the unmodulated swept carrier. The signal  $d(t)$  to noise  $m(t)$  ratio was 9.68dB. The recovered sweeping signal  $v'(t)$ , proportional to the instantaneous carrier frequency is shown in Figure 6.3. The maximum and minimum values of  $v'(t)$  correspond to the carrier frequencies of 65kHz and 95kHz respectively. The interfering signal has a frequency of 95 kHz and is observed as distortion in the corresponding level of  $v'(t)$ . This result clearly demonstrates the Phase-Locked Loop's behaviour as a bandpass tracking filter.

A similar test was conducted for a modulated carrier.



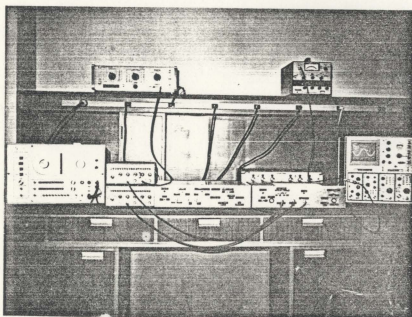


Figure 6.2b Laboratory Set-up of the Swept Carrier Multipath Channel Simulator

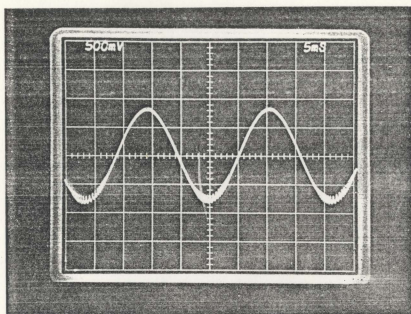


Figure 6.3 Recovered Sweeping Signal  $v'(t)$  showing Distortion associated with Interfering Tone

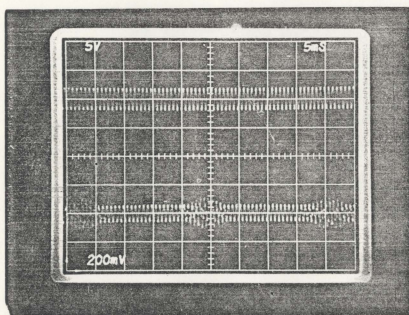


Figure 6.4 Transmitted Message  $x(t)$  (upper trace) and Recovered Message (lower trace) showing Distortion associated with Interfering Tone

Figure 6.4 shows a transmitted and demodulated message signal  $x(t)$  (upper trace) and  $x'(t)$  (lower trace), respectively, after removal of the low frequency sweeping waveform  $v'(t)$ . The periodical distortion is again caused by an interfering signal of 95kHz.

Using the Swept Carrier Multipath Channel Simulator, described in Section 6.2, quantitative measurements were obtained which demonstrate the system's ability regarding multipath suppression. Maintaining constant average multipath power, the normalized average noise power  $P$  at the FM demodulator output is shown in Figure 6.5 plotted against angle  $\phi$  with  $M$  as a parameter. The results are summarized in Table 6.1. As expected, for multipath spectrum widths of 10kHz and 30kHz, noise suppression is maximum as  $\phi$  approaches  $180^\circ$ . Figure 6.6 shows the photographs of the recovered sweeping signal for  $\phi = 0^\circ$  and  $180^\circ$  for  $M=10\text{kHz}$ . The periodic interference occurring around 80kHz for  $\phi = 180^\circ$  results from the interaction between the multipath spectrum  $F_m(\omega, t)$  and the tracking filter. For  $\phi = 0^\circ$ , there is no frequency separation between tracking filter bandwidth and multipath spectrum. The result is the interference which covers the entire recovered sweeping waveform  $v'(t)$ . Recovered message signal  $x'(t)$  for  $\phi = 0^\circ$  and  $\phi = 180^\circ$  for  $M=10\text{kHz}$  is shown in Figure 6.7. For  $\phi = 0^\circ$ , distortion affects the entire message signal. An improvement in  $x'(t)$  is obvious for  $\phi = 180^\circ$  where distortion is periodic.

For  $M=100\text{kHz}$ , the tracking filter is unable to

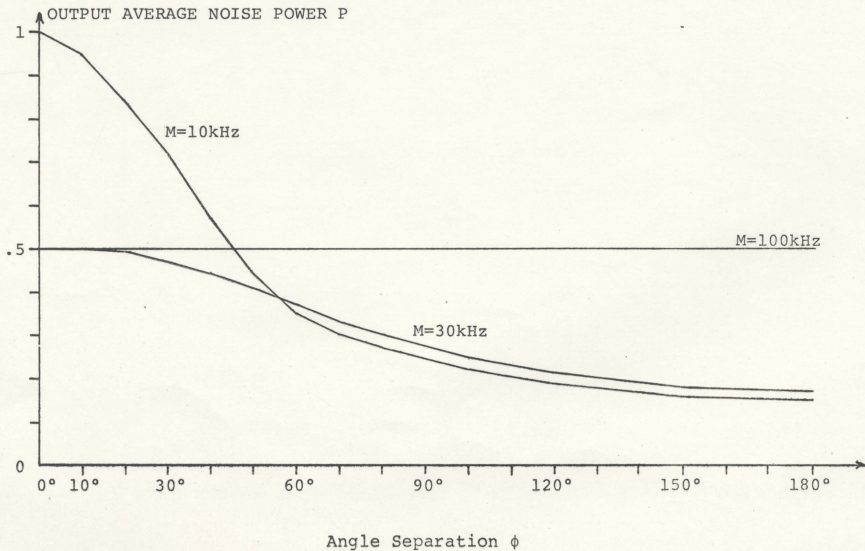


Figure 6.5 Normalized Average Noise Power  $P$  at the FM Demodulator Output vs Angle Separation  $\phi$  for  $M=10\text{kHz}$ ,  $30\text{kHz}$  and  $100\text{kHz}$

TABLE 6.1 Lab Results showing the Dependence of P on angle  $\phi$  (Figure 6.5)

Signal  $d(t)$  to noise  $m(t)$  ratio is 9.68dB

noise Bandwidth M	P													
	$\omega v=0^\circ$	$\phi=0^\circ$	$\phi=10^\circ$	$\phi=20^\circ$	$\phi=30^\circ$	$\phi=40^\circ$	$\phi=50^\circ$	$\phi=60^\circ$	$\phi=70^\circ$	$\phi=80^\circ$	$\phi=100^\circ$	$\phi=120^\circ$	$\phi=150^\circ$	$\phi=180^\circ$
10kHz	1	1	0.95	0.84	0.73	0.57	0.44	0.35	0.30	0.27	0.22	0.19	0.16	0.15
30kHz	0.50	0.50	0.50	0.49	0.47	0.44	0.40	0.37	0.33	0.30	0.24	0.21	0.18	0.17
100kHz	0.50	0.50	0.50	0.50	0.50	0.50	0.50	0.50	0.50	0.50	0.50	0.50	0.50	0.50

Remarks:

P is set equal to unity for the highest value of output average noise power. All other values are referred to this value.

The noise bandwidth of 100kHz covers the entire system operational range. The noise power within this range was equal to the noise power for bandwidths of 10kHz and 30kHz.

For  $\phi=0^\circ$ , P for 10kHz noise bandwidth is higher than P for noise bandwidth of 30kHz due to mechanism 2 of Chapter III. For  $\phi=180^\circ$ , P for 10kHz noise bandwidth is lower than P for 30kHz noise bandwidth due to mechanism 1 of Chapter III.



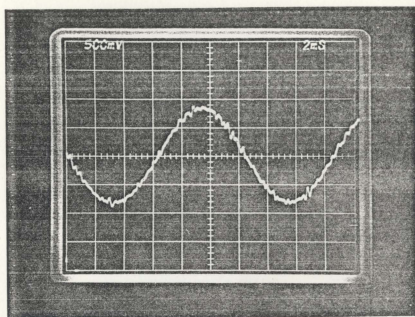


Figure 6.6a Recovered Sweeping Waveform  $v'(t)$  for  $\phi=0^\circ$ ,  $M=10\text{kHz}$

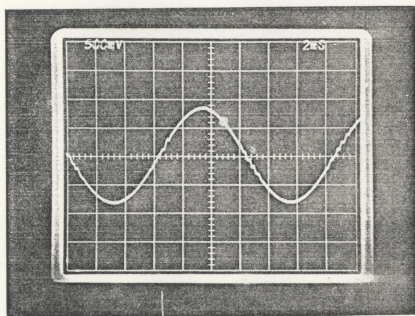


Figure 6.6b Recovered Sweeping Waveform  $v'(t)$  for  $\phi=180^\circ$ ,  $M=10\text{kHz}$



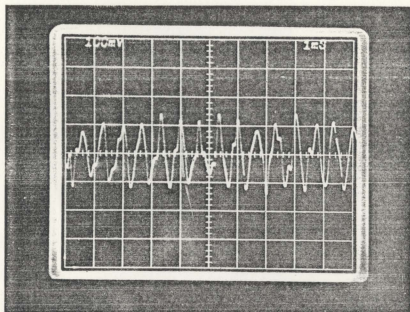


Figure 6.7a Recovered Message Signal  $x'(t)$  for a Frequency Modulated Swept Carrier,  $\phi=0^\circ$ ,  $\Delta M=10\text{kHz}$

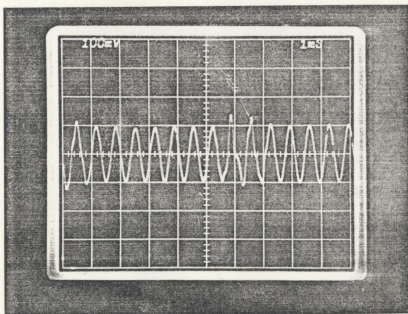


Figure 6.7b Recovered Message Signal  $x'(t)$  for a Frequency Modulated Swept Carrier,  $\phi=180^\circ$ ,  $\Delta M=10\text{kHz}$

"escape" from the presence of multipath. The result, seen in Figure 6.5, is a constant average value for noise power. These results, summarized in Table 6.1, back up the computer evaluation of Chapter IV.

#### 6.4 Tank and Sea Experiments

The functional block diagram of the system prototype is shown in Figure 6.8. An additional preamplifier stage and matching transformer was required during sea trials to counter effects produced by the long length of cable used. The transducers used in the experiments were omnidirectional. Related electrical schematics and specifications are contained in Appendix C.

Limited tests have been carried out in a small water tank. Due to the dimensions of the tank (3.7 x 3.7 x 3.7m.), strong and long lasting multipath was encountered. Figure 6.9 shows the received signal structure (lower trace) for the transmitted harmonic burst (upper trace). Even under these severe multipath conditions, the recovered sweeping waveform  $v'(t)$  was well defined as shown in Figure 6.10.

Sea trials were conducted in May 1978 during CSS "Hudson" cruise #78012. The geometry of the experiment is shown in Figure 6.11. The received signal structure (lower trace) for the transmitted high frequency pulse (upper trace) of 5 msec. duration is shown in Figure 6.12. The time delay  $\tau$  separating direct and multipath returns was approximately 17

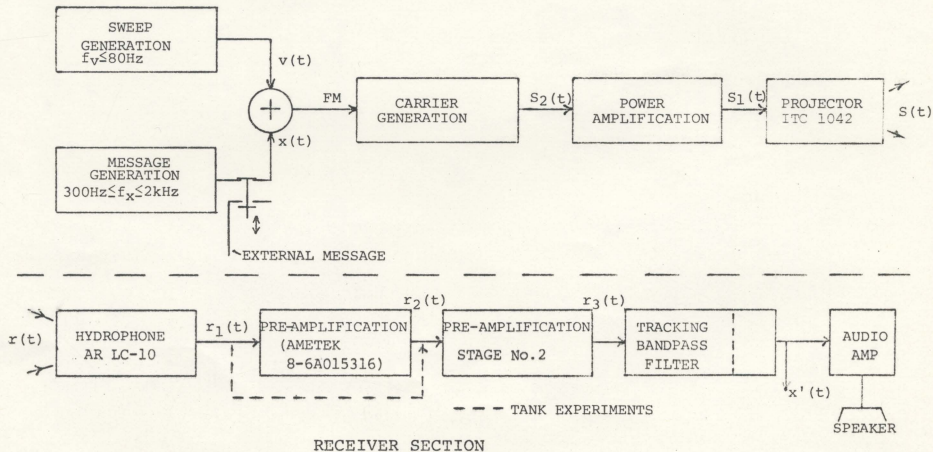


Figure 6.8 Function Block Diagram of System Prototype

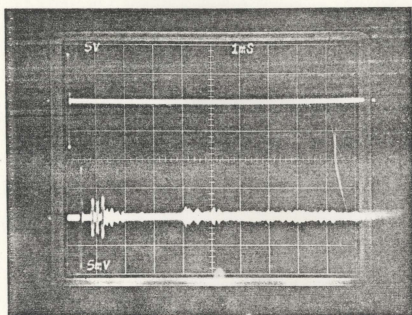


Figure 6.9 Transmitted (upper trace) and received (lower trace) signals

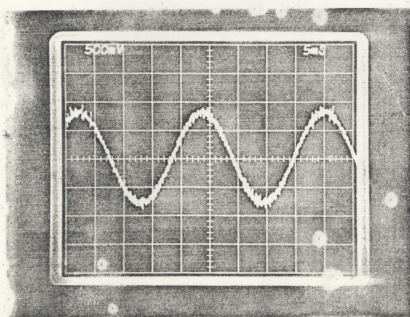


Figure 6.10 Recovered sweeping waveform  $v'(t)$

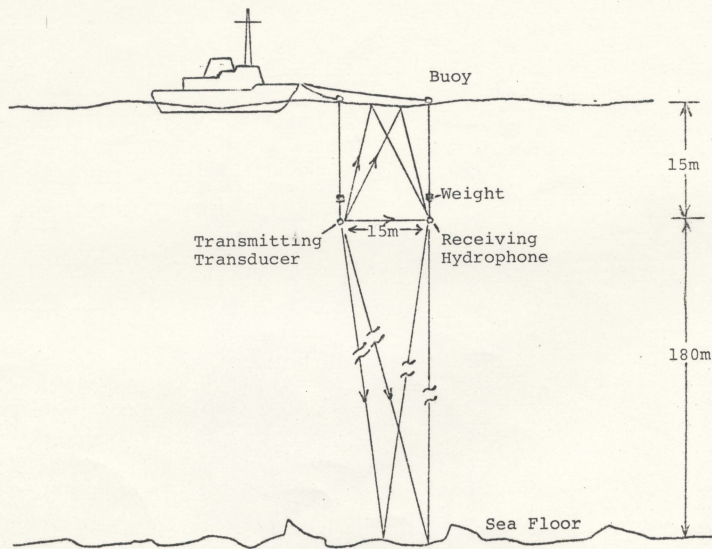


Figure 6.11 Geometry Associated with Sea Trials



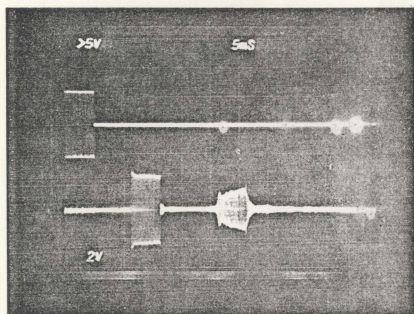


Figure 6.12 Transmitted (upper trace) and Received (lower trace) signals



msecs., while the multipath duration time  $T$  was 1 msec. For these values of  $\tau$  and  $T$ , the optimum sweeping frequency  $f_v$  as indicated by equation (3.16) for  $\phi=180^\circ$  is 29Hz. Figure 6.13a shows the received signal  $r(t)$  (upper trace) and recovered sweeping signal  $v'(t)$  (lower trace) for  $\phi=180^\circ$ . The departure from the optimum value of  $f_v$  results in increased distortion of the recovered sweeping waveform as indicated in Figure 6.13b where  $f_v=9\text{Hz}$  corresponding to  $\phi=110^\circ$ .

A similar experiment was conducted with the transmission of a sinusoidal message signal  $x(t)$ . Figure 6.14a<sup>1</sup> shows the recovered message signal  $x'(t)$  after the low frequency sweeping signal ( $f_v=29\text{Hz}$ ) has been filtered out. For comparison, Figure 6.14b shows the recovered message signal  $x'(t)$  obtained by conventional FM (unswept FM) transmission. An improvement over conventional FM with respect to amplitude fluctuation is evident.

<sup>1</sup>These photographs of Figure 6.14 were generated from a tape recording made of experiments. The signal levels are not representative of the deviation of the carrier by the message signal.

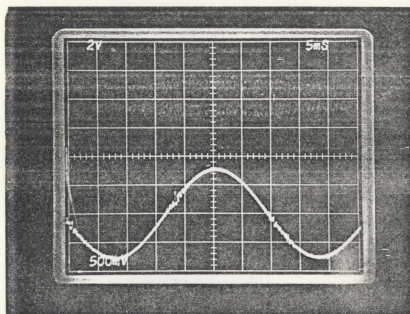


Figure 6.13a Received signal  $r(t)$  (upper trace) and Recovered Sweeping Signal  $v'(t)$  (lower trace) for  $\phi=180^\circ$

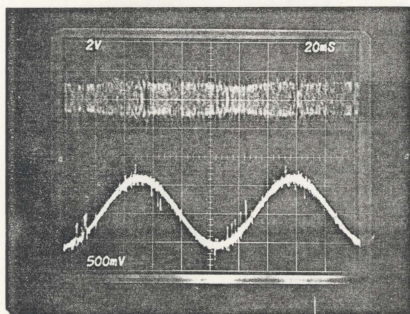


Figure 6.13b Received Signal  $r(t)$  (upper trace) and Recovered Sweeping Signal  $v'(t)$  (lower trace) for  $\phi=110^\circ$

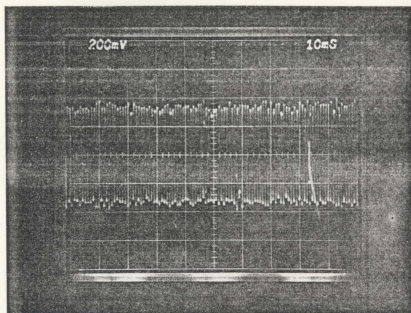


Figure 6.14a Recovered Message Signal for Swept Carrier Transmission,  $\phi=180^\circ$

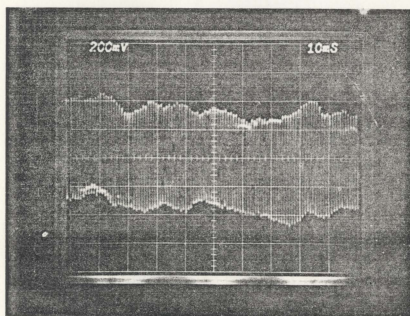


Figure 6.14b Recovered Message Signal for Classical FM Transmission

## CHAPTER VII

### CONCLUSIONS AND FURTHER WORK

In this thesis, an idea has been presented and developed for dealing with the problem of multipath interference in underwater acoustic communication systems. The research conducted is the initial step towards the development of a complete working system.

The simplified model developed in Chapter III was intended to expose essential features of the proposed swept carrier concept. Further work should be directed towards developing a more adequate mathematical model which would consider the duration, shape and intensity of the multipath spectrum associated with a swept carrier.

Further work is necessary concerning message modulation schemes available. Of the two considered, amplitude modulation and narrowband frequency modulation, there is a little difference with respect to bandwidth occupied by signal.

The sweeping waveform which controls the instantaneous frequency of the carrier is another area for consideration. The type of waveform employed to control the carrier frequency will obviously determine system performance and design.

A major area for further research is in receiver design. The main disadvantage of the Phase-Locked Loop acting as a tracking filter is the limited order of the loop. A second order loop for the receiver was considered in this

thesis. A higher order Phase-Locked Loop is desirable but would create serious design problems due to potential instability [5]. A possible frame work to follow in receiver design is seen in Figure 5.1. Obviously, from this figure, the implementation of the demodulator depends entirely on the message modulation scheme employed. Improvement in receiver design lies in evaluating the various arrangements which would compose the tracking bandpass filter.

Finally, the author would like to reiterate that the concept developed and tested in this thesis is the first step in a new direction aimed towards suppression of multipath in underwater acoustic communication systems. Further work, as outlined, is necessary before the development of a working system prototype is realized.



## BIBLIOGRAPHY AND LIST OF REFERENCES

1. Abotteen, R.A.: Probability of Error of a Binary Infinite Impulse Train Signal over a Random Parallel Channel. IEEE Transactions on Sonics and Ultrasonics. Vol. SU-25. March 1978.
2. Anderson, V.C.: Acoustic Communication is better than none. IEEE Spectrum. October 1970.
3. Andrews, R.S., and L.F. Turner: On the Performance of Underwater Data Transmission Systems using Amplitude-Shift-Keying Techniques. IEEE Transactions on Sonics and Ultrasonics. Vol. SU-23. January 1976.
4. Barbour, R.L., and A. Zielinski: Design of an Underwater Communication System. Internal Report No. N00119, Memorial University of Newfoundland. 1977.
5. Blanchard, A.: Phase-Locked Loops; Application to Coherent Receiver Design. New York: John Wiley & Sons, 1976.
6. Bohman, C.E., and D.E. Jackson: Underwater Acoustic Communication. Sperry Tech. Vol. 1, 1973.
7. Carlson, A.B.: Communication Systems; An Introduction to Signals and Noise in Electrical Communication. New York: McGraw Hill, 1968.
8. Cassara, F.A., T.S. Sundresh, and H. Schachter: Suppression of Interchannel Interference in FM Receiver.



Canadian Conference on Communication and Power, 1976.

9. Chancery, S.M. and C.E. Bohman: An Experiment in High Speed Underwater Telemetry. IEEE Int. Conference on Engineering in the Ocean Environment. New Port, R.I. 1972.
10. Downing, J.J.: Modulation Systems and Noise. N.J.: Prentice Hall, 1964.
11. Enloe, L.H.: Decreasing the Threshold in FM by Frequency Feedback. Proceedings of the IRE. January 1962.
12. Fortuin, L.: The Sea Surface as a Random Filter for Underwater Sound Waves. Ph.D. Thesis, Vitgeverij Waltman, Delft, 1973.
13. Gardner, F.M.: Phase-Locked Loop Techniques. New York: John Wiley and Sons, 1966.
14. Gerjuoy, E. and A. Yaspan: Physics of Sound in the Sea; Reverberation. New York: Gordon and Breach, 1968.
15. Goddard, G.C.: An Underwater Acoustic Telemeter for use in a Multipath Channel. Ph.D. Thesis, University of Birmingham. April 1970.
16. Hummels, D.R.: The Capacity of a Model for the Underwater Acoustic Channel. IEEE Trans. on Sonics and Ultrasonics, Vol. SU-19. July 1972.
17. Kinsler, L.E. and A.R. Frey: Fundamentals of Acoustics.

New York, N.Y.: John Wiley and Sons, 1962.

18. Knudsen, V.O., R.S. Alford and J.W. Emling: Underwater Ambient Noise. J. Marine Res., November 1948.
19. Lee, Y.W.: Statistical Theory of Communication. New York, N.Y.: John Wiley and Sons, 1960.
20. Lytle, D.W.: Characteristic Problems of the Underwater Channel. IEEE International Conference on Communications, Vol. 2. Seattle, Washington 1973.
21. Mackenzie, K.V.: Acoustic Behaviour of Near Bottom Sources Utilized for Navigation of Manned Deep Submergence Vehicles. Marine Tech. Soc. J., March 1969.
22. Morse, R.W.: Dependence of Shadow Zone Sound on the Surface Sound Velocity Gradient. J. Acoust. Soc. Am., Vol. 22, 1950.
23. Moschytz, G.S.: Miniaturized RC Filters Using Phase-Locked Loop. The Bell System Technical J., May, 1965.
24. Riter, S.: Underwater Acoustic Telemetry. Offshore Technology Conference. Dallas, Texas, 1970.
25. Riter, S. and P.A. Boatright: Design considerations for a Pulse Modulation Underwater Acoustic Communication System. IEEE International Conference on Engineering in the Ocean Environment, 1970.
26. Roberts, J.H.: Angle Modulation; The Theory of System

Assessment. London, U.K.: Peter Peregrinus, 1977.

27. Sakrison, D.J.: Communication Theory; Transmission of Waveforms and Digital Information. New York, N.Y.: John Wiley and Sons, 1968.
28. Schulkin, M. and H.W. Marsh: Absorption of Sound in Sea Water. J. Acoustic Soc. Am., Vol. 20, 1963.
29. Schwartz, M.: Information Transmission, Modulation, and Noise. New York, N.Y.: McGraw-Hill, 1959.
30. Steere, D.C.: Underwater Communication System for use by Free Swimming Divers. Master's Thesis # ADA013483, Naval Post Graduate School. Monterey, California.
31. Thorp, W.H.: Deep Ocean Sound Attenuation in the Sub and Low Kilocycle per second Region. J. Acoust. Soc. Am., Vol. 38, 1965.
32. Tucker, D.G. and B.K. Gazey: Applied Underwater Acoustics. London, U.K.: Pergamon Press, 1966.
33. Tuteur, F.B. and R.C. Spindel: Propagation and Communications through Underwater Acoustic Channels. Yale University, Microfiche AD717678, 1970.
34. Urick, R.J.: Principles of Underwater Sound. New York, N.Y.: McGraw-Hill, 1967.
35. Venetsanopoulos, A.W.: Stochastic Filter Modeling for the Sea-Surface Scattering Channel. J. Acoust. Soc.

Am., Vol. 49, April 1971.

36. Walpole, R.E. and R.H. Myres: Probability and Statistics for Engineers and Scientists. New York, N.Y.: MacMillan Co., 1972.
37. Whalen, A.D.: Detection of Signals in Noise. New York, N.Y.: Academic Press, 1971.
38. Williscroft, R.G. and N.C. Macleod: A Non-Acoustic Long Distance Underwater Communication System. IEEE MTS Conference, Washington (D.C.), September 1978.
39. Zielinski, A. and R.L. Barbour: Swept Carrier Acoustic Underwater Communications. IEEE MTS Conference, Washington, (D.C.), September 1978.
40. Zielinski, A. and R.L. Barbour: The Swept Carrier Underwater Acoustic Communication System. 5th International Ocean Development Conference, Tokyo, Japan, September, 1978.

APPENDIX A  
COMPUTER SIMULATION PROGRAM

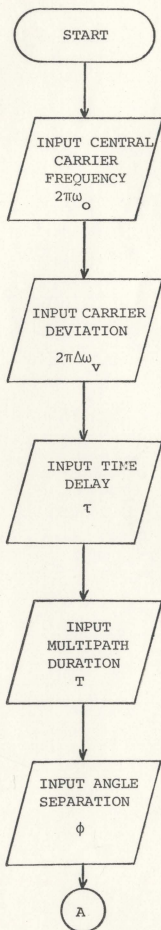
The computer simulation implemented in Chapter IV provides an analysis of the performance of a swept carrier system pertaining to its multipath suppression capability.

The program, developed on the mini HP9825A computer and HP9862A calculator plotter can be used for any receiver transfer function  $K(\omega, t)$ . It will output if desired, plots of noise power vs time and noise density vs time at the receiver's output. The program is general such that

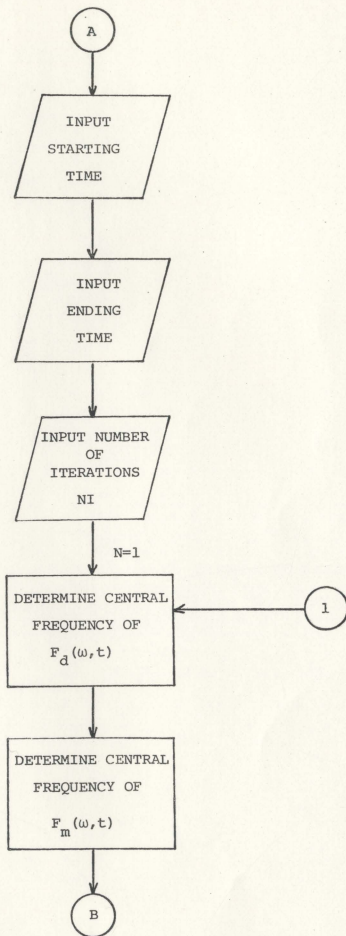
- a) any receiver transfer function  $K(\omega, t)$  can be implemented
- and
- b) central carrier frequency  $F_o$ , carrier sweep range  $f_{\min}$  to  $f_{\max}$ , multipath parameters  $\tau$  and  $T$ , and desired angle separation  $\phi$  are inputted by the user.

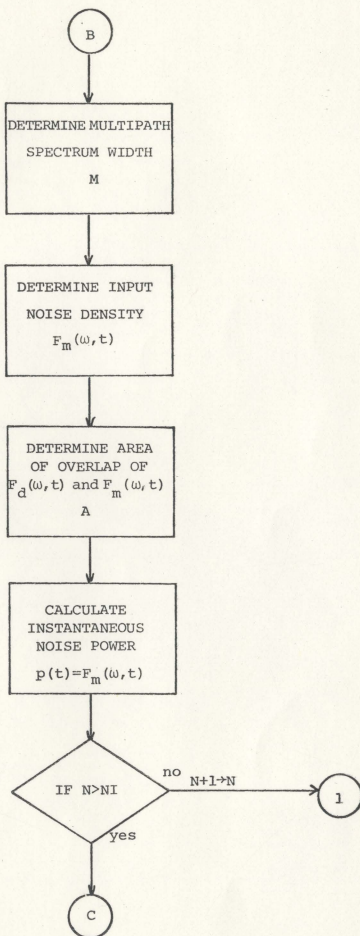
A listing of the program and associated flowchart follows.

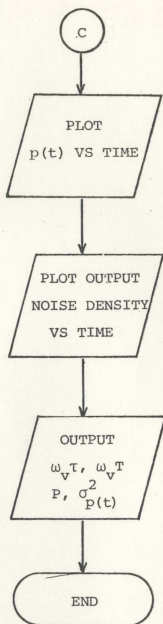












```

0: enp "START-0,
  INTERIM-1,END-
  2",A;sto 4
1: avd
2: 0→J
3: 1→A
4: if A=1;sto
  128
5: if A=2;sto
  155
6: dim V[20],
  W[10],C[20],
  U[2],K[15],X[0:
  8],E[2]
7: rad
8: flt 7
9: enp "FILTER
  CUT OFF FREQ",
  E,"FILTER ORDER
  ",0
10: enp "VCO
  FREE RUN",V[1],
  "CARRIER DEV",
  V[2]
11: 5→R[7]
12: .00001→R[15]
13: 1→Z
14: prt "MULTIPAR
  TH CONDITIONS
  EXISTING ARE"
15: enp "DELAY
  D-M?",V[5],"M
  DURATION?",V[6]
16:  $\pi/(V[5]+V[6]
  /2)+C[3]$ 
17: prt "OPTIMUM
  SWEEP FREQ
  FOR 180 DEG
  SEPARATION IS",
  C[3]/(2 $\pi$ );prt
  "Hz"
18: enp "DESIRED
  ANG SEP,< $\pi$ --0,
  = $\pi$ --1",B
19: if B=1; $\pi$ →V[7]
  ;sto 23

```

```

20: enp "ANG
  SEP?",V[7]
21: V[7]/(V[5]+
  V[6]/2)+C[3]
22: prt "SWEEPIN
  G FREQ=",C[3]/
  (2 $\pi$ )
23: 2 $\pi$ /C[3]→C[4]
  J
24: spc 3
25: prt "Period
  =",C[4]
26: spc 3
27: enp "START
  TIME",W[1],"END
  TIME",W[2]
28: enp "STEPS",
  W[3],"NOPRT-0,
  PRT-1",W[4]
29: if A=1;sto
  31
30: dim P[W[3]+
  1],G[W[3]+1],
  T[W[3]+1],F[W[3]
  +1]
31: (W[2]-W[1])/
  W[3]→C[5]
32: 1→N
33: W[1]→T[N]
34: 0→C
35: 1→V
36: 0→C[2]
37: V[1]+V[2]*
  cos(C[3]*T[N]-
   $\pi/2$ )→C[6]
38: V[1]+V[2]*
  cos(C[3]*T[N]-
  V[7]- $\pi/2$ )→C[7]
39: V[1]+V[2]*
  cos(C[3]*T[N]-
  C[3]*V[5]-C[3]*
  V[6]- $\pi/2$ )→U[1]
40: V[1]+V[2]*
  cos(C[3]*T[N]-
  C[3]*V[5]- $\pi/
  2$ )→U[2]
41: if C[3]*V[6]
  > $\pi$ ;sto 58
42: if C=1;sto
  48

```

```

43: (V[7]+C[3]*
    V[6]/2)*180/
    π+V[8]
44: (V[7]-C[3]*
    V[6]/2)*180/
    π+V[9]
45: if C=0;if
    V[9]<90;if V[8]
    >90;sto 52
46: if C=0;if
    V[9]<270;if
    V[8]>270;sto 54
47: sto 56
48: if U[2]>Y;
    if U[1]>X;sto
    56
49: if U[2]<Y;
    if U[1]>X;sto
    54
50: if U[2]<Y;
    if U[1]<X;sto
    56
51: if U[2]>Y;
    if U[1]<X
52: Z/abs(max(U[
    *])- (V[1]-V[2])
    )+G[N];max(U[*
    ])+E[2];V[1]-
    V[2]+E[1]
53: 3+H;sto 78
54: Z/abs(min(U[
    *])- (V[1]+V[2])
    )+G[N];min(U[*
    ])+E[2];V[1]+
    V[2]+E[1]
55: 2+H;sto 78
56: Z/abs(U[1]-
    U[2])+G[N];U[1]
    +E[1];U[2]+E[2]
    ;1+H
57: sto 78
58: if C=1;sto
    69
59: if V[7]≠π;
    if V[7]<2*π;
    sto 65
60: if V[7]>=2*
    π;V[7]-2*π+V[7]
61: (V[7]+C[3]*
    V[6]/2+2*(π-
    C[3]*V[6]/2))*
    180/π+V[8]

```

```

62: (V[7]+C[3]*
    V[6]/2)*180/
    π+V[9]
63: if C=0;if
    V[8]>270;if
    V[9]<270;sto 73
64: sto 77
65: (V[7]-C[3]*
    V[6]/2-2*(π-
    C[3]*V[6]/2))*
    180/π+V[8]
66: (V[7]-C[3]*
    V[6]/2)*180/
    π+V[9]
67: if C=0;if
    V[8]<90;if V[9]
    >90;sto 75
68: sto 77
69: if U[1]<X;
    if U[2]<Y;sto
    77
70: if U[1]>X;
    if U[2]<Y;sto
    75
71: if U[1]>X;
    if U[2]>Y;sto
    77
72: if U[1]<X;
    if U[2]>Y
73: Z/(max(U[*
    ])- (V[1]-V[2]))
    +G[N];V[1]-V[2]
    +E[1];max(U[*
    ])+E[2]
74: 6+H;sto 78
75: Z/(V[1]+V[2]
    -min(U[*]))+G[N]
    ;V[1]+V[2]+E[1]
    ;min(U[*])+E[2]
    ]
76: 5+H;sto 78
77: Z/(2*V[2])+G
    [N];V[1]-V[2]+E
    [1];V[1]+V[2]+E
    [2];4+H
78: C[6]+F[N]
79: if E[1]>E[2]
    ;E[1]+R[2];E[2]
    +R[1]
80: if E[1]<E[2]
    ;E[2]+R[2];E[1]
    +R[1]

```

```

81:  asb "ROMBERG
    "
82:  if W[4]=1;
    prt "ISD(F)=",
    G[N]
83:  X[0]*G[N]→P[
    N]
84:  P[N]/abs(E[2
    ]-E[1])+G[N]
85:  if W[4]=0;
    sto 92
86:  spc
87:  prt "C[7]=",
    C[7];prt "U[1]=
    ",U[1];prt "U[2
    ]=",U[2]
88:  prt "MULTP
    SPECTRUM POSITI
    ON=",H
89:  prt "FREQ=",
    F[N];prt "OSD(F
    )=",G[N]
90:  prt "TIME=",
    T[N];prt "P(t)=
    ",P[N]
91:  spc
92:  C[2]+P[N]→C[
    2]
93:  dsp "STEP
    NO.",V
94:  V+1→V
95:  U[1]→X;U[2]→
    Y
96:  1→C
97:  if N-1<W[3];
    N+1→N;T[N-1]→
    C[5]→T[N];sto
    37
98:  spc
99:  prt "MAX
    STEPS =",N
100: spc 4
101: flt 5
102: if S=1;prt
    "FILE NO.",Q;
    spc
103: prt "WsD=",
    C[3]*V[5];spc
104: prt "WsT=",
    C[3]*V[6];spc

```

```

105: if V[7]/π*
    180<=180;prt
    "ANG SEP=",V[7]
    /π*180;spc
106: if V[7]/π*
    180>180;prt
    "ANG SEP=",abs(
    360-V[7]/π*180)
    ;SPC
107: prt "Averag
    e Noise Power="
    ;C[2]/(W[3]+1)
108: C[2]/(W[3]+
    1)→C[8]
109: spc
110: prt "Energy
    of Output Nois
    e per Sweep=",
    C[8]*C[4]
111: spc
112: 1→N
113: 0→C[17]
114: (P[N]-C[8])
    →C[19]
115: C[17]+C[19]
    →C[17];N+1→N;
    if N<=W[3]+1;
    sto 114
116: C[17]/(W[3]
    +1)→C[18]
117: prt "VAR",
    C[18]
118: spc
119: prt "STD.
    DEV.",rc[C[18]
120: spc
121: prt "Max
    Dev from Averag
    e=",(max(P[*])-
    C[8])/rc[C[18];
    prt "Std. Dev.'
    s"
122: spc
123: prt "Min
    Dev from Averag
    e=",(min(P[*])-
    C[8])/rc[C[18];
    prt "Std. Dev.'
    s"
124: spc 4
125: fxd 7
126: ldf 3

```



```

127: spc
128: flt 7
129: enp "NEW
MULTP CONDITION
S ? NO-0;YES-
1",V[3]
130: if V[3]=0;
sto 155
131: spc
132: prt "CHANGE
PEN";sto 14;
stp
133: "ROMBERG":c
fa 2;if R[1]>R[
2];sfa 2;dsp
"BOUNDS REVERSE
D";ret
134: 0+R[3];R[1]
+R[4];esb 153
135: R[5]+R[3]+R
[3];R[2]+R[4];
esb 153
136: R[5]+R[3]+R
[3];((R[2]-R[1]
)/2)R[3]+X[0];
0+R[6]
137: if (R[6]+
1+R[6])>R[7];
sto +7
138: ((2+((R[6]-
1)+R[8])+R[9])-
1+R[10]
139: -1+R[11];
0+R[3]
140: if (R[11]+
2+R[11])<=R[10]
;sto 142
141: (((R[2]-
R[1])/R[8])R[3]
+X[R[6]-1])/
2+X[R[6]];sto -
4
142: R[1]+((R[2]
-R[1])/R[9])R[1]
1]+R[4];esb 153
143: R[3]+R[5]+R
[3];sto -3
144: 1+R[12]
145: if (R[12]+
1+R[12])>R[7]+
1;ret
146: -1+R[6];
sfa 6

```

```

147: if (R[6]+
1+R[6])>R[7]+1-
R[12];sto -2
148: X[R[6]]+R[1]
3]
149: ((4+(R[12]-
1)+R[14])X[R[6]
+1]-X[R[6]])/
(R[14]-1)+X[R[6]
]]
150: if flg6;
cfa 6;sto -3
151: if abs(R[13]
1-X[R[6]])<R[15]
1;X[R[6]]+X[0];
ret
152: sto -5
153: (1+((R[4]-
C[6])/E)+((2*
0))+(-1/2))+2+R[
5]
154: ret
155: end
*13150

```

## PLOTING PROGRAM

```

0: flt 6
1: prt "MAX VAL
  OF P[N]=";max(P
  [N]);"MAX VAL
  OF G[N]=";max(G
  [N])
2: enp "UPPER
  LIMIT OF POWER"
  ,P
3: enp "UPPER
  LIMIT OF OUTPUT
  NOISE DENSITY"
  ,G
4: enp "Labellin
  g? Yes-1;No-
  0",U
5: W[3]+1+N
6: scl -T[N]/10;
  T[N]+T[N]/30;-
  .2*P,1.2*P;csiz
  2.5,2,1/2,0
7: if A=1;prt
  "CHANGE SCALE";
  sto
8: if U=0;sto 20
9: plt (T[N]-
  T[1])/W[3]*(2*
  W[3]/13);1.1*P;
  1
10: lbl "PLOT
  OF OUTPUT NOISE
  POWER P(t) vs
  TIME FOR ONE
  PERIOD OF V(T)"
11: deg
12: csiz 2.5,2;
  1/2,90
13: plt T[1]-
  T[N]/12,.1*P,1
14: lbl "OUTPUT
  NOISE POWER
  P(t)-watts"
15: csiz 2.5,2;
  1/2,0
16: plt (T[N]-
  T[1])/W[3]*(2*
  W[3]/6);-.2*P,1
17: lbl "TIME
  (T)-ONE PERIOD
  OF V(T)"
18: rad
19: flt 2
20: axe 0,0,T[N]
  /(8*(T[N]/C[4])
  ),P/10
21: if U=0;sto
  36
22: csiz 2,2,1/
  2,0
23: 2*P/10+Y
24: plt 0,Y,1
25: celt -9,.2
26: lbl Y
27: Y+2*P/10+Y
28: if Y<=P;sto
  24
29: csiz 2,2,1/
  2,0
30: T[N]/(8*T[N]
  /C[4])X
31: 1/8+Z
32: plt X,0,1
33: celt -9,-1
34: lbl Z
35: if X<=max(T[
  N]);Z+1/8+Z;X+
  T[N]/(8*(T[N]/
  C[4]))X;sto 32
36: 1+N
37: plt T[N];
  P[N]
38: if N<=W[3];
  N+1+N;sto 37
39: pen
40: 1+N
41: plt T[N];
  C[2]/(W[3]+1)
42: if N<=W[3];
  N+1+N;sto 41
43: pen
44: enp "MIN
  STEP",X;"MAX
  STEP",Y
45: scl -T[Y]/
  10,T[Y]+T[Y]/
  30;-.2*G,1.2*G;
  csiz 2.5,2,1/2,
  0

```

```

46: if A=0:prt
  "CHANGE SCALE";
  sto 48:stp
47: if A=1:prt
  "CHANGE SCALE";
  stp
48: if U=0:sto
  59
49: plt (T[Y]-
  T[X])/W[3]*(2*
  W[3]/10.5),1.1*
  G,1
50: lbl "PLOT
  OF OUTPUT NOISE
  DENSITY Gno(f,
  t) vs ONE PERIO
  D OF V(T)"
51: des
52: csiz 2.5,2,
  1/2,90
53: plt T[X]-
  T[Y]/12,.1*G,1
54: lbl "OUTPUT
  NOISE DENSITY
  Gno-V*V/Hz"
55: csiz 2.5,2,
  1/2,0
56: plt (T[Y]-
  T[X])/W[3]*(2*
  W[3]/6),-.2*G,1
57: lbl "TIME
  (t)-ONE PERIOD
  OF V(Y)"
58: rad
59: axe 0,0,T[N]
  /(8*(T[N]/C[4])
  ),G/10
60: if U=0:sto
  80
61: csiz 2,2,1/
  2,0
62: 2*G/10+J
63: plt 0,J,1
64: cplt -9,.2
65: lbl J
66: J+2*G/10+J
67: if J<=G:sto
  63
68: csiz 2,2,1/
  2,0

```

```

69: T[N]/(8*T[N]
  /C[4])K
70: 1/8+R
71: fxd 2
72: plt K,0,1
73: cplt -10,-1
74: lbl (V[1]+
  V[2]*cos(C[3]*
  K-p/2))/1000,"
  KHz"
75: f1t 2
76: plt K,0,1
77: cplt -9,-2.5
78: lbl R
79: if K<=max(T[
  N]);R+1/8+R;K+
  T[N]/(8*T[N]/
  C[4])+K;sto 71
80: X+N
81: plt T[N],
  G[N]
82: if N<Y;N+
  1+N;sto 81
83: pen
84: end
*23747

```

## APPENDIX B

### DESIGN CONSIDERATIONS FOR THE EXPERIMENTAL SYSTEM RECEIVER

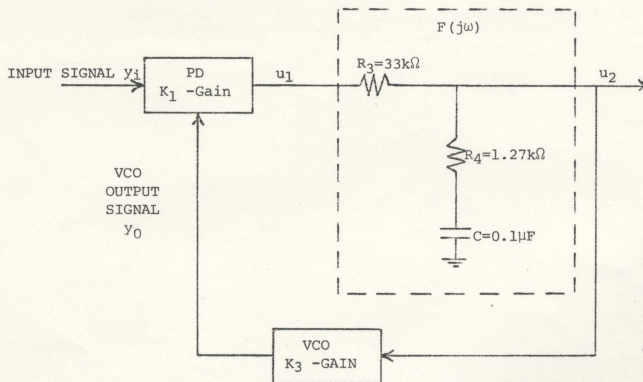
The functional block diagram of a Phase-Locked Loop (PLL) is shown in Figure 6.1. The loop used in the experimental system receiver was second order with low pass filter and phase lead correction as shown in Figure B1. Of the various types of loops that could be used, the second order loop with low pass filter and phase lead correction provides the independent choice of two essential parameters, namely the natural angular frequency  $\omega_n$  and the damping factor  $\xi$ , when the loop gain  $K$  is otherwise given. The three independent parameters available using this loop will enable the loop to perform simultaneously as a tracking filter and frequency demodulator.

A high gain ( $K=4.5 \times 10^5$  rad/s) phase-locked loop (RCA CD-4046) is used to perform the tracking and frequency demodulation function. The loop filter's transfer function is expressed as

$$F(j\omega) = \frac{1 + T_1 j\omega}{1 + T_2 j\omega} \quad (B1)$$

where time constants  $T_1$  and  $T_2$  are represented as  $(R_3+R_4)C$  and  $R_4C$  respectively. The transfer function of the loop is given by

$$H(j) = \frac{\omega_n^2 + j(2\xi\omega_n - \omega_n^2/K)\omega}{\omega_n^2 - \omega^2 + j2\xi\omega_n\omega} \quad (B2)$$



Loop Gain  $K_1 K_3 = K = 4.32 (10^5) \text{ rad/s}$   

$$F(j\omega) = \frac{1 + T_1 j\omega}{1 + T_2 j\omega}$$

$$T_1 = (R_3 + R_4)C = 3.43 \text{ ms}$$

$$T_2 = R_4 C = 130 \mu\text{s}$$

$$\omega_n = 1.12 (10^4) \text{ rad/s}$$

$$\xi = 0.726$$

$$B_r = 6000 \text{ Hz}$$

Figure B1 Model of a Second Order Phase-Locked Loop  
 Working as a Tracking Bandpass Filter  
 (RCA CD-4046)

where the natural angular frequency  $\omega_n$  is related to  $K$  and  $T_1$  by

$$\omega_n^2 = \frac{K}{T_1} \quad (B3)$$

and damping factor  $\xi$  by

$$2\xi\omega_n = \frac{1 + KT_1}{T_1} \quad (B4)$$

The time constants  $T_1$  and  $T_2$  are so chosen that  $\omega_n = 1.12(10^4)$  rad/s and  $\xi=0.726$  ( $T_1=3.43$ ms,  $T_2=130$ ns). A damping factor of  $\xi=0.726$  ensures minimum loop noise bandwidth while high loop gain ( $K=4.5 \times 10^5$  rad/s) ensures good tracking.

The amplitude-frequency characteristic for this loop is shown in Figure B2 [5] and expressed as

$$|H(j\omega)| = \left[ \frac{1 + (2\xi - \omega_n/K)^2 x^2}{(1 + x^2)^2 + 4\xi^2 x^2} \right]^{1/2} \quad (B5)$$

The -3dB bandwidth obtained using (B5) is  $1.7\omega_n/2\pi=3$ kHz, the overshoot of the response curve is +3.86dB and the asymptotic slope is -6dB/octave (Figure B2). The tracking filter bandwidth is twice the -3dB bandwidth and expressed as  $B_r$ .



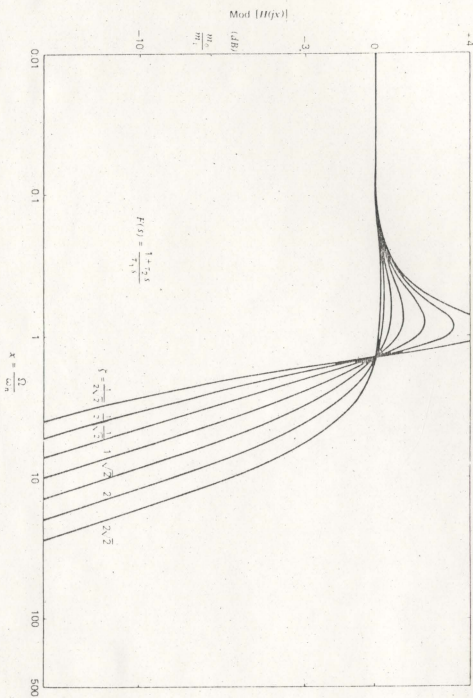


Figure B2 Transfer function of a second-order loop with  $F(s) = (1 + 2.8/s)/(s^2 + 2.8s)$ ; amplitude-frequency characteristic [5]

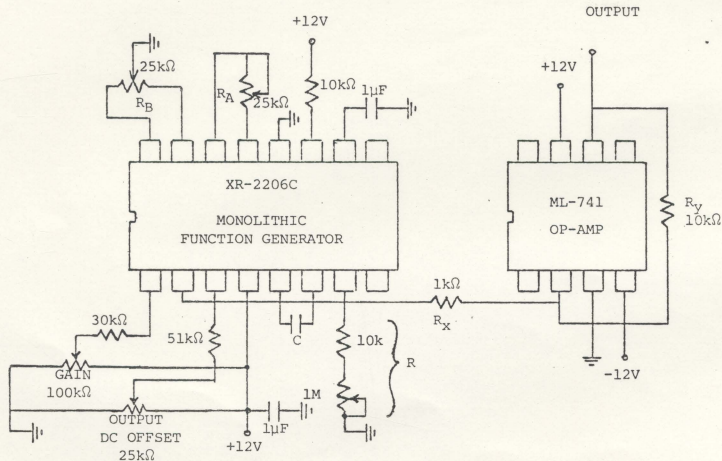
## APPENDIX C

### RELATED SYSTEM SCHEMATICS AND SPECIFICATIONS

The system prototype was designed for a test range of 100 meters. The threshold requirements necessary for the Phase-Locked Loop in the system's receiver require a signal to noise<sup>1</sup> ratio of greater than 6dB. The numerical design considerations which determine the required transmitter power to overcome transmission losses and noise levels to achieve this 6dB S/N ratio have been outlined in 4 . The prototype was designed to have a S/N ratio of approximately 50dB over a 100 meter test range. Such a ratio means the deterioration of the signal caused by ambient and thermal noise is negligible. Additional pre-amplification at the receiver is designed to provide any further desired amplification while minimizing noise introduced by receiver electronics.

The remainder of this appendix is comprised of the electrical schematics and specifications associated with the functional block diagram of the system prototype (Figure 6.8).

<sup>1</sup>This noise level results from the sea's ambient noise and thermal noise caused by molecular agitation.



$R_A$  - WAVEFORM SYMMETRY

$R_B$  - WAVEFORM SHAPING

$$v(t) = A_v \cos 2\pi f_v t$$

$$A_v = (\text{GAIN}) (R_Y / R_X)$$

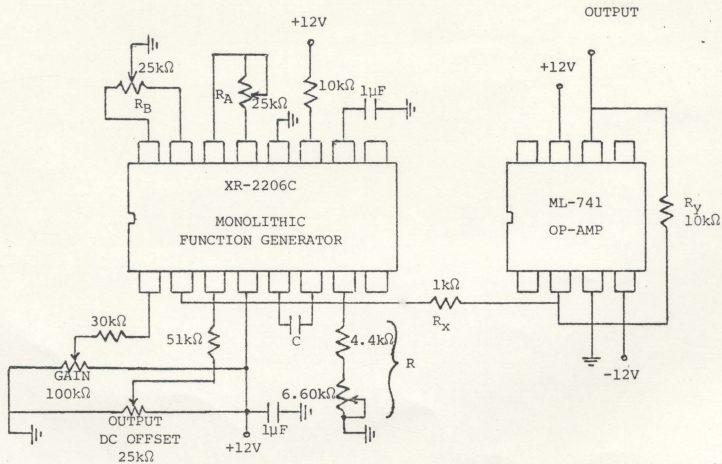
$$1\text{Hz} \leq f_v \leq 100\text{Hz}$$

$$f_v = \frac{1}{RC}$$

$$10\text{k}\Omega \leq R \leq 1\text{M}\Omega$$

$$C = 1\mu\text{F}$$

Figure C1 Sweep Generation



$R_A$  - WAVEFORM SUMMETRY

$R_B$  - WAVEFORM SHAPING

$$x(t) = A_x \cos 2\pi f_x t$$

$$A_x = (\text{GAIN}) (R_Y / R_x)$$

$$300\text{Hz} \leq f_x \leq 2\text{kHz}$$

$$f_v = \frac{1}{RC}$$

$$4.4\text{k}\Omega \leq R \leq 660\text{k}\Omega$$

$$C = 0.22\mu\text{F}$$

Figure C2 Message Generation

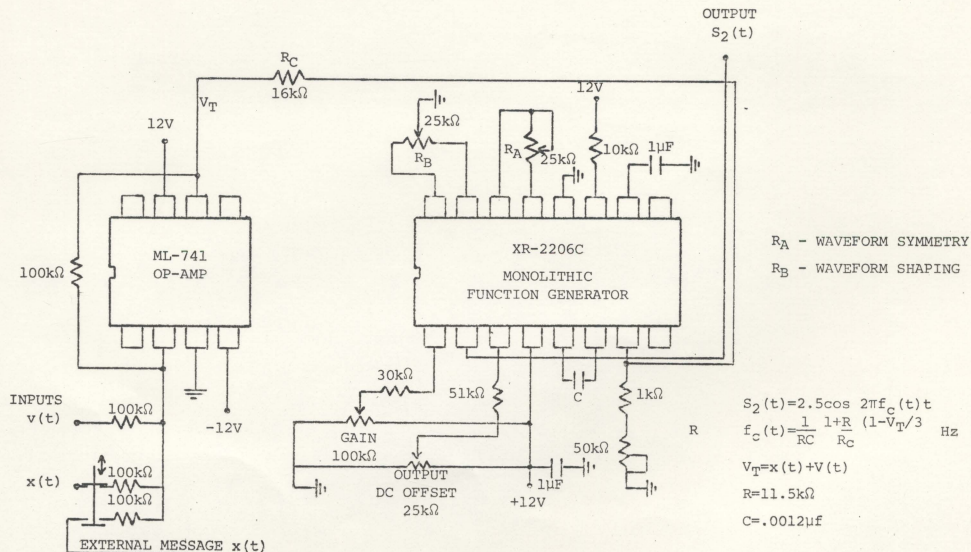


Figure C3 Carrier Generation

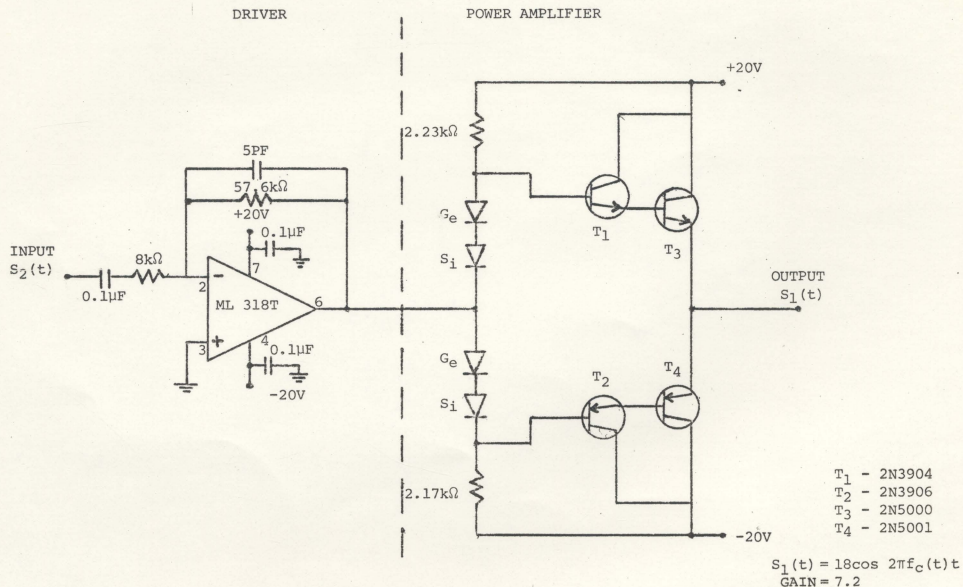


Figure C4 Power Amplification



INTERNATIONAL TRANSDUCER CORP.

Voltage Source Level

ITC No. 1042 Serial No. 093

OPERATOR RFJ

Date 3-4-77

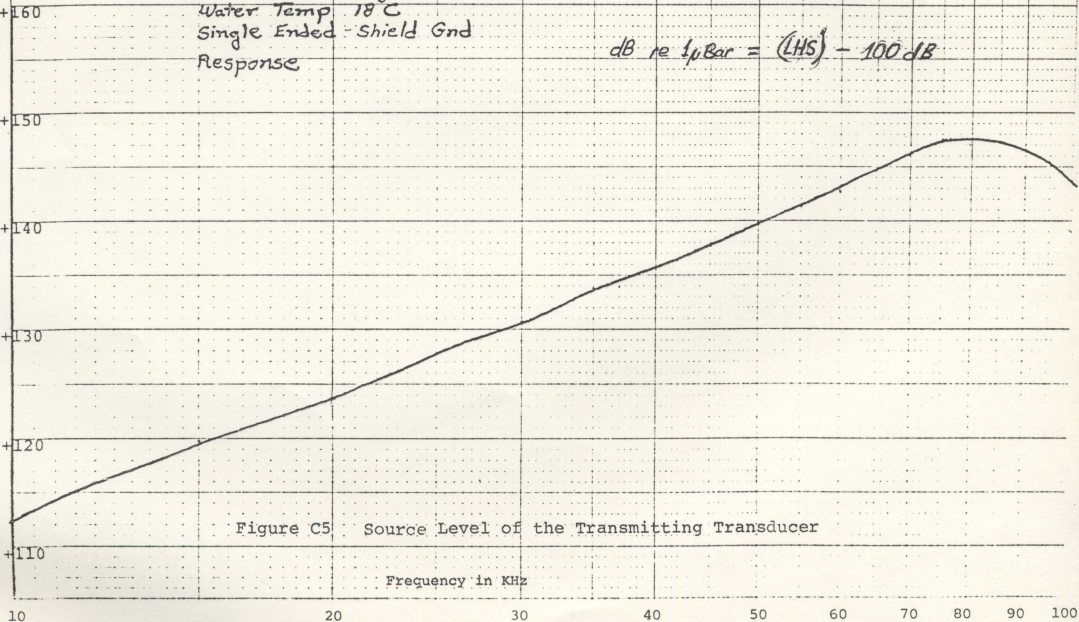
Water Temp 18°C  
Single Ended - Shield Gnd  
Response

dB re 1  $\mu$ Bar = (LHS) - 100 dB

dB re 1  $\mu$ Pa . m/V

Figure C5 Source Level of the Transmitting Transducer

Frequency in KHz



# LC-10

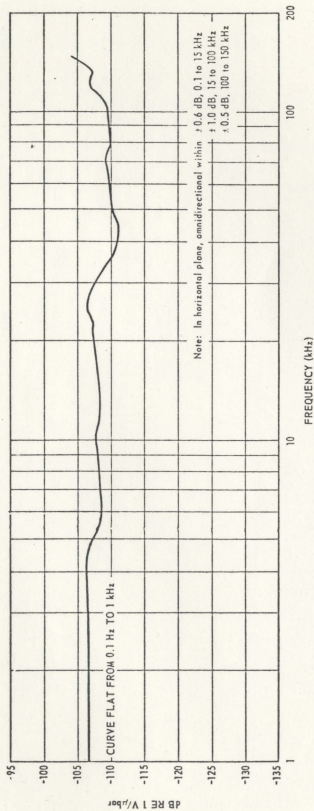


Figure C6 Typical free-field voltage sensitivity, the LC-10 hydrophone open-circuit voltage at end of 25-foot coaxial cable.

NOTE The first pre-amplification stage as indicated in Figure 6.8 utilized an Ametek 8-6A015316 pre-amplifier

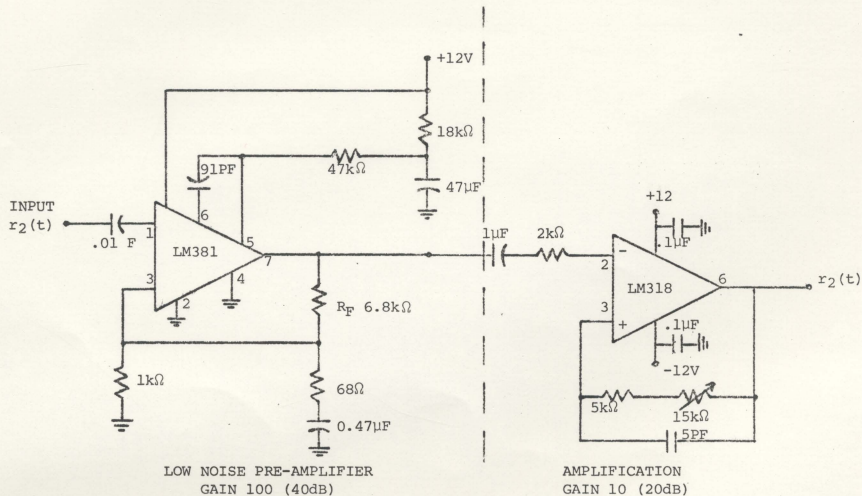


Figure C7 Pre-amplification Stage No.2

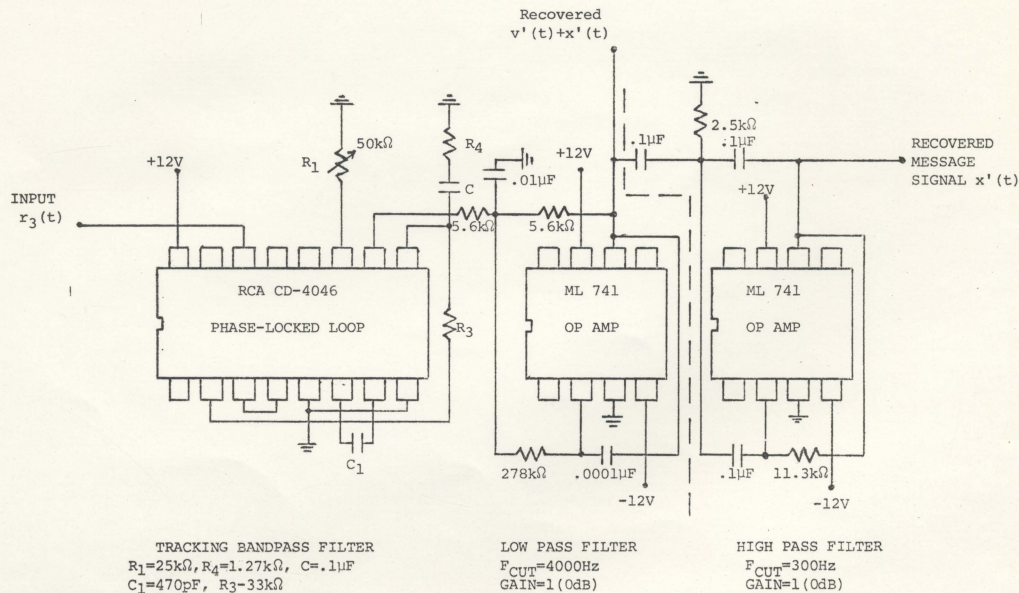


Figure C8 Tracking BandPass Filter and Frequency Demodulator

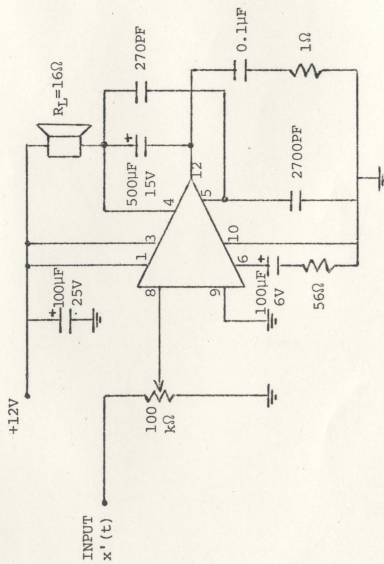


Figure C9 Audio Amplifier







